

AN ANALYTICAL AND EXPERIMENTAL
INVESTIGATION OF STRESS DISTRIBUTION
IN THE PUNCHED METAL PLATE
OF A TIMBER JOINT

Thesis for the Degree of Ph. D.
MICHIGAN STATE UNIVERSITY
Ram Daur Misra
1964

This is to certify that the

thesis entitled

An Analytical and Experimental
Investigation of Stress Distribution
in the Punched Metal Plate of a
Timber Joint.
presented by

Ram D. Misra

has been accepted towards fulfillment
of the requirements for

Ph.D. degree in Agricultural Engineering

F H Beelaw

Major professor

Date March 2, 1964



MS

ABSTRACT

AN ANALYTICAL AND EXPERIMENTAL INVESTIGATION OF STRESS DISTRIBUTION IN THE PUNCHED METAL PLATE OF A TIMBER JOINT

by Ram Daur Misra

The main objective of this study was to conduct a theoretical and experimental investigation of stress distribution in a punched metal plate of a timber joint.

The theoretical investigation consisted of two different methods. One utilized the discrete approach of a difference equation while the other used the continuous approach of the principle of minimum complementary energy.

A second order difference equation was derived and solved for a general case. The results for the particular case of the metal plate connector were calculated and plotted together with the experimental results for comparison.

The principle of minimum complementary energy was used to derive a second order ordinary linear differential equation for an idealized case. The metal plate connector was treated as if glued to the surface of the wood by a fictitious adhesive of negligible thickness. The differential equation thus obtained was solved with appropriate boundary conditions. The results for the particular case of metal plate connector were plotted with the experimental results for comparison.

Two different methods of experimental stress analysis were used; namely, PhotoStress analysis and a strain gage technique.

The PhotoStress analysis provided, qualitatively, the overall pattern of stress distribution in the entire plate. A set of bar graphs for the principal stress difference ($\sigma_1 - \sigma_2$) along the various rows of the teeth in the metal plate connector were plotted. A symmetrical stress distribution was obtained. The isoclinic pattern for a portion of the plate was thoroughly examined. From this isoclinic pattern stress trajectories were drawn.

The strain gage technique was used to obtain accurate and reliable values of strain in the metal plate to verify the theoretical results.

From the results of this investigation the following conclusions and observations were made.

1. The results of the difference equation solution as well as that of the principle of minimum complementary energy predict reasonable agreement with the experimental results. Either method can be used to calculate stresses in the metal plate connector.
2. The difference equation solution can also be used with at least equal accuracy for riveted and bolted joints. Similarly the results of the principle of minimum complementary energy are equally applicable for adhesive as well as welded joints.
3. The stresses in the metal plate are not uniform as assumed in the normal design practices. The maximum calculated stress in the connector was 2.4 times the average value.
4. A set of destruction tests made in tension resulted in tearing failure of the plate in the center of the joint. If the middle part of the plate were not punched, the strength of the joint should be greater and also a more uniform stress distribution should result.

5. The PhotoStress analysis provided an overall pattern of stress distribution in the entire plate. The variation between measured and calculated principal stress difference ranged from 9.6% to 42.2%. The results of this analysis were, however, incomplete as the shape of the punched plate was too complicated for analytical separation of the principal stresses. The equipment for experimental separation (oblique incidence meter) was not available.

Approved *F H BueLOW*
Major Professor

AN ANALYTICAL AND EXPERIMENTAL INVESTIGATION
OF STRESS DISTRIBUTION IN THE PUNCHED METAL
PLATE OF A TIMBER JOINT

By

Ram Daur Misra

A THESIS

Submitted to
Michigan State University
in partial fulfillment of the requirements
for the degree of

DOCTOR OF PHILOSOPHY

Department of Agricultural Engineering

1964

3 21111
1-23-65

ACKNOWLEDGMENTS

I wish to express my sincere thanks to Dr. F. H. Buelow, chairman of the guidance committee, for his pleasant counsel and many helpful suggestions. Sincere thanks are also expressed to Drs. J. S. Boyd and M. L. Esmay, ex-chairmen, for their inspiring guidance and constant supervision of this project.

I am greatly indebted to Dr. A. W. Farrall, chairman, Department of Agricultural Engineering for making available the research assistantship which enabled me to undertake this study. The financial support of Troy Steel Corporation for this project is gratefully acknowledged.

Grateful appreciation is expressed to the other members of the guidance committee; Dr. L. E. Malvern (Metallurgy, Mechanics and Material Science), Dr. R. K. Wen (Civil Engineering) and Dr. B. F. Cargill (Agricultural Engineering) for their guidance, suggestions and interest in this project.

Special thanks are due to Dr. C. A. Tatro, formerly of the Department of Metallurgy, Mechanics and Material Science for his continual help in the experimental work.

The assistance of Mr. J. B. Cawood and his associates of the Research Laboratory in mechanical construction and in supplying the necessary tools and equipment is duly recognized.

TABLE OF CONTENTS

	Page
INTRODUCTION	1
Objective	2
REVIEW OF LITERATURE	3
Timber Joints Connected by Metal Plates	3
Analysis of Joints	4
PhotoStress Analysis	6
THEORETICAL INVESTIGATION	8
Analysis by Means of a Difference Equation	8
Solution of the Difference Equation	12
Analysis by the Principle of Minimum Complementary Energy	15
Derivation of Differential Equation	18
Solution of the Differential Equation	21
EXPERIMENTAL INVESTIGATION	23
PhotoStress Analysis	23
Test Specimen	24
Testing Procedure	27
Results and Discussion of PhotoStress Analysis . .	27
Stress Magnitudes	27
Stress Directions	34
Isoclinics	34
Stress Trajectories (Isostatics)	36
Strain Gage Analysis	38
Test Specimen	38
Testing Procedure	39
Results and Discussion of Strain Gage Analysis . .	39
RESULTS AND DISCUSSION	51

TABLE OF CONTENTS - Continued

	Page
Comparison of Theoretical and Experimental Results. .	51
Evaluation of PhotoStress Analysis	55
SUMMARY	58
CONCLUSIONS AND OBSERVATIONS	60
SUGGESTIONS FOR FURTHER STUDY.	60a
REFERENCES	61

LIST OF TABLES

TABLE	Page
I. Principal Stress Differences at a Network of Points in the Metal Plate Connector, Loaded in Tension. (System of Point Designation is Shown in Figure 5). . .	29
II. Comparison of Measured and Calculated Stresses on Strips Along Row 7 at a Tensile Load of 2500 lbs Per Plate	34

LIST OF FIGURES

FIGURE	Page
1. Schematic drawing of the metal plate connected timber joint.	9
2. Deformed metal plate connector and the variation of force F as it increases from 0 at $x = 0$ to P at $x = np$. .	11
3. Actual and idealized joints used in the analysis.	17
4. Equilibrium of small elements across the idealized joint	17
5. Shape of the punched teeth in the metal plate connector and location of strain gages	25
6. Test specimen and principal stress difference variation along columns 2 and 5.	26
7. Test apparatus for PhotoStress study	28
8. Test apparatus for strain gage investigation	28
9. Histogram representation of principal stress differences along columns 1 and 2.	31
10. Histogram representation of principal stress differences along columns 3 and 4	32
11. Histogram representation of principal stress differences along columns 5 and 6	33
12. Isoclinics in the metal plate connector, loaded in tension (The location of this portion on the plate is shown in Figure 5)	35
13. Stress trajectories in the metal plate connector, loaded in tension.	37

LIST OF FIGURES - Continued

FIGURE	Page
14. Load stress curves for points (1, 1), (1, 3), (1, 5) and (1, 7)	40
15. Load stress curves for points (2, 1), (2, 3), (2, 5) and (2, 7)	41
16. Load stress curves for points (3, 1), (3, 3), (3, 5) and (3, 7)	42
17. Load stress curves for points (4, 1), (4, 3), (4, 5) and (4, 7)	43
18. Load stress curves for points (5, 1), (5, 3), (5, 5) and (5, 7)	44
19. Load stress curves for points (6, 1), (6, 3), (6, 5) . . .	45
20. Stress distribution in the metal plate connector at 5,000 lbs tension	47
21. Stress distribution in the metal plate connector at 5,000 lbs tension	48
22. Stresses at the bases of cantilever teeth in the metal plate connector at 5,000 lbs tension	49
23. Stresses at the bases of cantilever teeth in the metal plate connector at 5,000 lbs tension	50
24. Comparison of experimental and theoretical results as predicted by the difference equation solution	52
25. Comparison of experimental and theoretical results as predicted by the principle of minimum complementary energy	54
26. Stress distribution in the metal plate connector as obtained from the analyses of the minimum complementary energy and the difference equation	56

INTRODUCTION

Wood trusses with spans of 20 to 40 feet have been used in the past 5 to 10 years for the construction of farm buildings, light storage structures and homes. A satisfactory and economical fastener to join the truss members continues to be the main problem in the design and development of light wood trusses.

Considerable research has been done on ring-bolt and glue-nail fasteners in the past few years. Both have limitations and disadvantages. Glue-nail fasteners, for example, cannot be used when the temperature is below freezing unless heated space is provided.

In recent years various types of metal plate connectors have been developed for wood trusses. These connectors are made from commercial quality galvanized steel sheets ranging in thickness from 14 to 20 gauge. The method of fastening varies widely from manufacturer to manufacturer. It may range from rectangular teeth punched and bent 90° to the face of the plate to simply holes drilled in the plate in which nails are later inserted. The length of these punched teeth may vary from 1/4 to 3/4 inch. The general acceptance and preliminary performance of these connectors indicate a potential for farm use as well as wider application in house construction.

There is a lack of basic information on the load transmitting characteristics of the metal plate connectors. A tangible and accurate method of analyzing and designing these connectors has not yet been developed. The stress distribution in a metal plate under field conditions or even idealized conditions of loading is not well-known. The design of the metal plate connectors is based on the assumption that there is a uniformly distributed load and that each tooth acts as a miniature

cantilever beam. Also, it is assumed that the load is constant over the entire length and the width of the plate. These assumptions seem to be rather general and inaccurate. A few preliminary tests made before the beginning of this project indicated a sharp stress gradient in the metal plate in the direction of loading.

This project was, therefore, undertaken to investigate accurately the stress distribution in a metal plate connector.

Objective

The objective of this investigation was to make a theoretical and experimental stress analysis of a metal-plate-connected timber joint in uniaxial tension.

REVIEW OF LITERATURE

Timber Joints Connected by Metal Plates

Felton (1963) conducted an extensive study to determine the design loading values for various types of standard metal truss plates. He attempted to establish design loading values as follows:

1. Load per tooth or nail.
2. Load per square inch of plate area.
3. Load per ounce of metal plate and its fastenings.

A total of eleven different types of plates were used for evaluating the performance of truss plate joints in tension and shear. Five replications of each test were made.

The test data were evaluated statistically by an analysis of variance. It was established that the shear joints gave higher values of ultimate loads than the tension joints.

The following conclusions may be drawn from his study:

1. The shear tests as used gave unrealistically high values for load carrying capacity of truss plates.
2. The tension test appears to give a realistic value for the load carrying capacity of truss plates.
3. The metal truss plates can be used to make satisfactory joints for trussed rafter construction.
4. The metal truss plates make relatively rigid joints.
5. Joints with a low net cross-sectional plate area failed in the plate rather than in the wood.
6. The 3/4" long rectangular teeth did not have a tendency to bend, but rather crushed the wood fibres on the sides toward the load application.
7. The smooth shanked nail had a tendency to bend and withdraw and to crush the wood fibres on the sides toward the load application.

It has been well-established that the timber joints connected with metal plates and nails slip with respect to wood when loaded. This is also an indication of the rigidity of these joints. The amount of slip increases with the magnitude of load as well as with accelerated aging.

Joy (1960) conducted a comprehensive study of metal plate connectors for wood trusses. He particularly investigated the slip characteristics of these connectors at different loads and a series of humidity conditions. A photographic record of load slip data was made. From this permanent record the average slip was plotted against load.

The study indicated that the slip of plates, loaded while aging, was very marked. At about half "Plastic Flow Start" load the slip of joints being aged was 2 to 5 times the slip of unaged units. The author accounts a part of this increase to humidity effect while the rest due to time alone or creep.

Analysis of Joints

It appears that there has been no attempt to analyze the metal-plate-connected timber joints analytically. The literature surveyed here deals primarily with the analysis of forces in riveted, bolted and welded connections. Certain similarities of these joints to metal plate connectors make it relevant to review these investigations.

Hrennikoff (1932) used the work of rivets in riveted joints to determine the distribution of load among various rivets. He divided his study into three parts. Part I consisted of a qualitative study with some observations on conventional design methods. Part II included the derivation of formulas in a few simple types of joints based on the assumption that a rivet develops a force proportional to deformation. In Part III the formulas of Part II were applied to the determination of the numerical values of the coefficients found analytically.

The author drew the following conclusions on the basis of his analysis.

1. The standard practice of dividing the force in proportion to the shearing areas of the rivets and disregarding the deformation of the plates leads to results that are very inaccurate.
2. Actually, the total force acting on a riveted joint is not distributed equally among the rivets; a larger portion of the total work is done by the outer rivets.
3. The proportion of the total work in the outer rivets increases as the pitch and diameter of the rivets increase and the cross-section of the plates decreases.
4. If there are many rivets in a longitudinal row, the inner rivets are inefficient, and an increase in the number does not improve the value of the joint appreciably.

Muckle (1949) used the principle of minimum strain energy to determine the distribution of load in riveted joints. He made the following assumptions for simplicity of his analysis.

1. The plate between any two rows of rivets is in a state of uniform stress; and
2. A portion or the whole of the shank of the rivet is in a state of uniform shear stress.

The investigation covered treble, quadruple and quintuple-riveted lapped joints, and treble-riveted double cover butt joints.

The author concluded that (except in double riveted joints) the load is not uniformly distributed over the various rows of rivets; the outer rows take more and the inner rows less than the average load. He further pointed out that because of the nature of assumptions made in developing the theory the results should be regarded as being qualitative only. The friction between plates, for instance, had been entirely ignored. The author also made an interesting observation: that except for treble-riveted lapped joints, the modulus of elasticity of the joints examined exceeded that of solid plate, and it is possible that, in practice, the modulus of elasticity would be greater in all cases. The reduced value

of modulus of elasticity in large riveted structures should not therefore be employed for calculations.

In the analysis of Hrennikoff and Muckle reviewed above, very laborious calculation is involved, and whenever the number of connectors is to be changed a new problem must be solved. To overcome this difficulty Harris (1962) used the difference equation approach for analyzing parallel-type structural connections.

Harris developed a second order difference equation relating the increment of force transmitted by connectors and the stiffness factors of members and connectors. The equation was solved by a trial and error process with appropriate boundary conditions. The results were plotted for various ratios of stiffness factors.

PhotoStress Analysis

PhotoStress is a trade name for the birefringent coating technique of experimental stress analysis. It is essentially a photoelastic technique except that no model analysis is required. The actual specimen to be stress analyzed is coated with a special transparent plastic that exhibits temporary birefringence (double refraction) when strained. This birefringence is directly proportional to the intensity of strain. When a polarized light is passed through the strained plastic, black and colored fringe patterns corresponding to the direction and intensity of principal strains can be observed and measured by a reflection polariscope. The black lines called isoclinics, connect points of the same principal stress direction on the specimen. The colored fringe patterns called isochromatics, connect points on the stressed specimen that have same magnitude of principal stress difference.

The effects of strain gradient and the curvature of the surface under load on the photoelastic pattern were studied by Duffy (1961).

He used a Fourier Series solution for the displacement to represent surface strain gradients for a one-dimensional problem. From his series solution he showed that the fringe order is directly proportional to surface strain only if strain is uniform or varies linearly with distance. In all other cases the results will be erroneous. Even for thin coating thicknesses errors may be as high as 35%.

He concluded that

Experimental results are influenced considerably by two factors not previously investigated; namely, a gradient in the strain at the metal surface, and the curvature of this surface under load. Neglecting either of these factors may lead to large errors and, under certain circumstances, it is possible for one or the other to produce a greater birefringence than does the surface strain.

Post and Zandman (1961) made an extensive study of effects of Poisson's ratio and coating thickness on the accuracy of PhotoStress technique. They made the following conclusions on the basis of their experimental investigation.

1. For the case of plane stress problems and equal Poisson's ratio of structure and coating, the influence of coating thickness on birefringence developed along free boundaries is almost identically zero.
2. For unequal Poisson's ratio and simply connected structures in plane stress, birefringence developed along free boundaries is almost exactly independent of coating thickness.
3. For simply connected structures in plane stress, very thick coatings behave essentially as independent bodies subjected to prescribed end displacements, i. e., as photoelastic models. In this case birefringence is independent of Poisson's ratio.
4. In order to minimize effects of dissimilar Poisson's ratio and local reinforcement, thin coatings are preferable. For most engineering problems 1/8 in. coating should be adequately thin.

THEORETICAL INVESTIGATION

The theoretical analysis of the metal plate connector was made by two different methods. One used the discrete approach of a difference equation while the other utilized the continuous approach of the principle of minimum complementary energy. The validity of these analyses, of course, depends upon the soundness of the assumptions underlying them and the mathematical limitations, as a theory describing a physical phenomenon can be no better than the assumptions on which it is based. Neither of these analyses can, therefore, be claimed to describe the exact physical behavior of the joint. They are only approximations to the actual behavior.

Analysis by Means of a Difference Equation

By definition, a difference equation relates the values of a function y and one or more of its differences $\Delta y, \Delta^2 y, \dots$ for each x -value of some set of numbers S (for which each of these functions is defined). Or, in brief, a difference equation is a relation involving differences.

The analysis made here by means of a difference equation is similar to one used by Harris (1962) for parallel-type structural connections.

The metal plate connected timber joint is shown schematically in Figure 1a. It consists of two punched metal plates driven into the wood, one on each face of the joint. Because of symmetry, it is sufficient to consider only a quarter portion of the joint for analysis. This part is shown in Figure 1b.

The load from member A, the wood part, is transmitted to member B, the metal plate, by connectors c . The force at any point

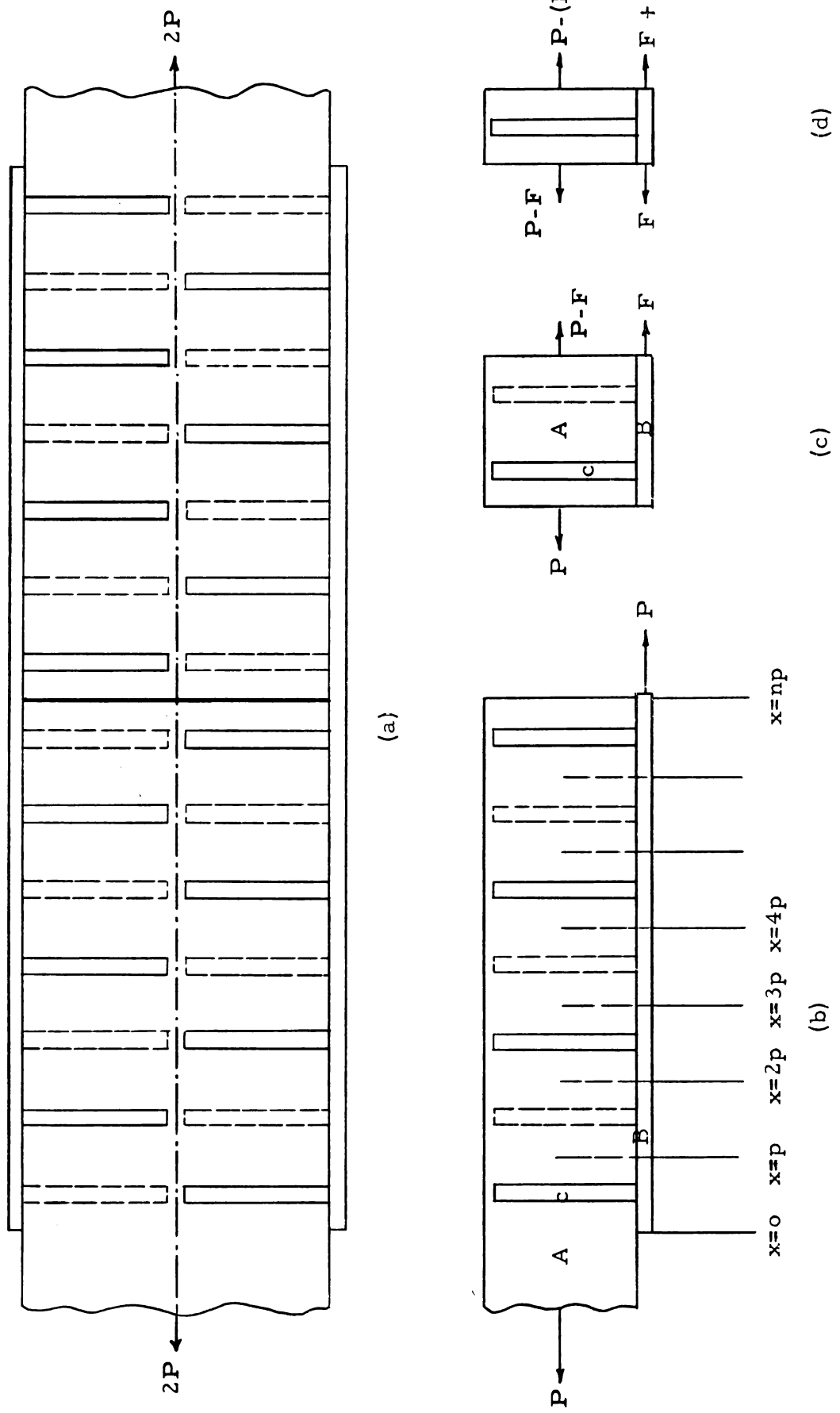


Fig. 1. Schematic drawing of the metal plate connected timber joint.

in member B is F and corresponding force in member A is $P-F$. Figure 2b shows the variation of force F in member B as it increases from 0 at $x = 0$ to P at $x = np$. The increase in F from F_{x-p} at $x = x-p$ to F_x at $x = x$ is the first difference of F , and is represented by $(\Delta F)_x$. Thus,

$$(\Delta F)_x = F_x - F_{x-p} \quad (1.1)$$

The second difference of F is

$$\begin{aligned} (\Delta^2 F)_x &= (\Delta F)_{x+p} - (\Delta F)_x & (1.2) \\ &= (F_{x+p} - F_x) - (F_x - F_{x-p}) \\ &= (F_{x+p} - 2F_x + F_{x-p}) \end{aligned}$$

or
$$(\Delta F)_{x+p} = (\Delta^2 F)_x + (\Delta F)_x$$

The smaller portion of the connector is shown in Figure 1d. Here, the force in the left-hand portion of member B is F and the force on the right-hand is $F+\Delta F$; the force transmitted by the connector is ΔF , which is the first difference of the force in member B.

Figure 2a, shows that the force in the left-hand connector c_1 is ΔF and the force in the right-hand connector c_2 is $\Delta F + \Delta^2 F$; where $\Delta^2 F$ is the second difference between forces on adjacent connectors. Supposing that k_1 and k_2 are the stiffness factors for connectors c_1 and c_2 respectively, the deformation of these two connectors can be expressed as follows,

$$\text{Deformation of connector } c_1 = \frac{\text{Force in } c_1}{\text{stiffness of } c_1} = \frac{\Delta F}{k_1}$$

$$\text{Deformation of connector } c_2 = \frac{\text{Force in } c_2}{\text{stiffness of } c_2} = \frac{\Delta F + \Delta^2 F}{k_2}$$

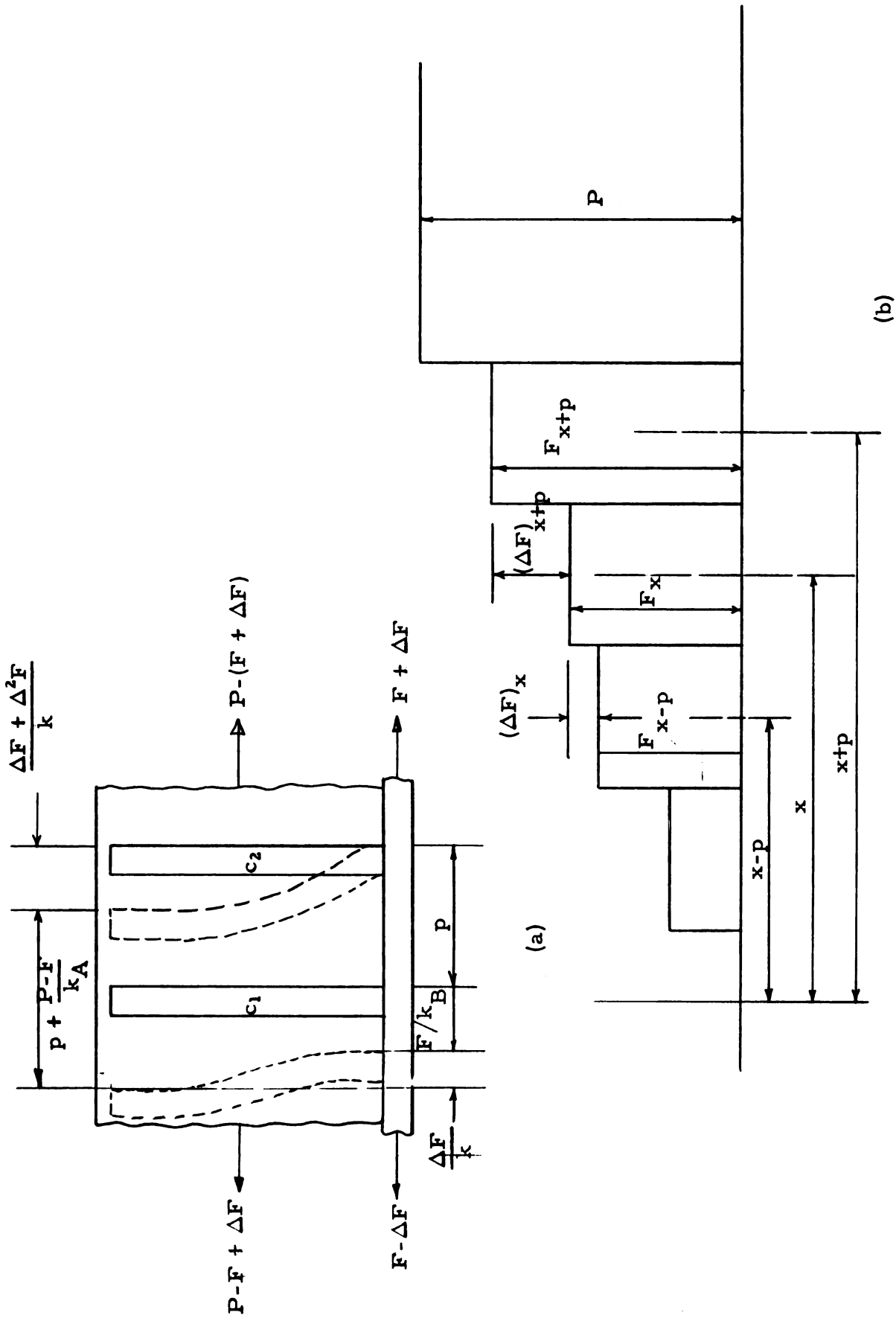


Fig. 2. Deformed metal plate connector and the variation of force F as it increases from 0 at $x = 0$ to P at $x = np$.

Again from Figure 2a it is seen that member A stretches by $(P-F)/k_A$ and member B stretches by F/k_B ; where k_A and k_B are the stiffness factors of members A and B respectively.

In addition to stretching of members A and B and deformation of connectors c_1 and c_2 , there is a relative slip between the wood and the metal plate. Assuming that this slip is negligible which implies that the joint is rigid; it must be then, that the sum of dimensions in upper part of the joint shown in Figure 2a less the sum of dimensions in the lower part must vanish, or mathematically

$$\left(\frac{\Delta F}{k_1} + \frac{F}{k_B}\right) - \left(\frac{P-F}{k_A} + \frac{\Delta F + \Delta^2 F}{k_2}\right) = 0 \quad (1.3)$$

Assuming that the connectors have the same stiffness factor (which they do in this case) $k_1 = k_2 = k$, Eq. (1.3) becomes

$$\frac{F}{k_B} - \frac{P-F}{k_A} - \frac{\Delta^2 F}{k} = 0$$

$$\text{or} \quad \Delta^2 F - (k/k_B)F + (k/k_A)(P-F) = 0 \quad (1.4)$$

$$\text{or} \quad \Delta^2 F - (k/k_A + k/k_B)F = - (k/k_A) P$$

$$\text{or} \quad \Delta^2 F - \omega^2 F = -\omega_1^2 P \quad (1.5)$$

where $(k/k_A + k/k_B) = \omega^2$ and $(k/k_A) = \omega_1^2$

Equation (1.5) above is a difference equation relating the force in member B to the total force P and the various stiffness factors.

Solution of the Difference Equation

The solution of the difference equation (1.5) may be broken down into two parts, analogous to ordinary differential equation theory; namely, the complementary solution and the particular solution.

The complementary solution of the difference equation (1.5) is the solution of the homogeneous difference equation

$$\Delta^2 F - \omega^2 F = 0 \quad (1.6)$$

To obtain the complementary solution one may use the method of trial. Keeping in mind the similarity of the difference equation (1.6) with certain ordinary linear differential equations, one may guess that the solution would be a combination of hyperbolic cosine and hyperbolic sine with two constants, as the difference equation is of second order. Supposing that

$$F = A \text{Cosh } mx, \quad \text{where } m = \text{an unknown constant}$$

then
$$\begin{aligned} (\Delta^2 F)_x &= F_{x+p} - 2F_x + F_{x-p} \\ &= A \text{Cosh } m(x+p) - 2A \text{Cosh } mx + A \text{Cosh } m(x-p). \end{aligned}$$

Substituting $\Delta^2 F$ and F into Eq. (1.6) gives

$$\begin{aligned} A \text{Cosh } m(x+p) - 2A \text{Cosh } mx + A \text{Cosh } m(x-p) - \omega^2 A \text{Cosh } \\ mx = 0 \end{aligned} \quad (1.7)$$

Using the identity

$\text{Cosh}(a \pm b) = \text{Cosh } a \text{Cosh } b \pm \text{Sinh } a \text{Sinh } b$ in Eq. (1.7) reduces it to:

$$2 \text{Cosh } mx \text{Cosh } mp - 2 \text{Cosh } mx - \omega^2 \text{Cosh } mx = 0$$

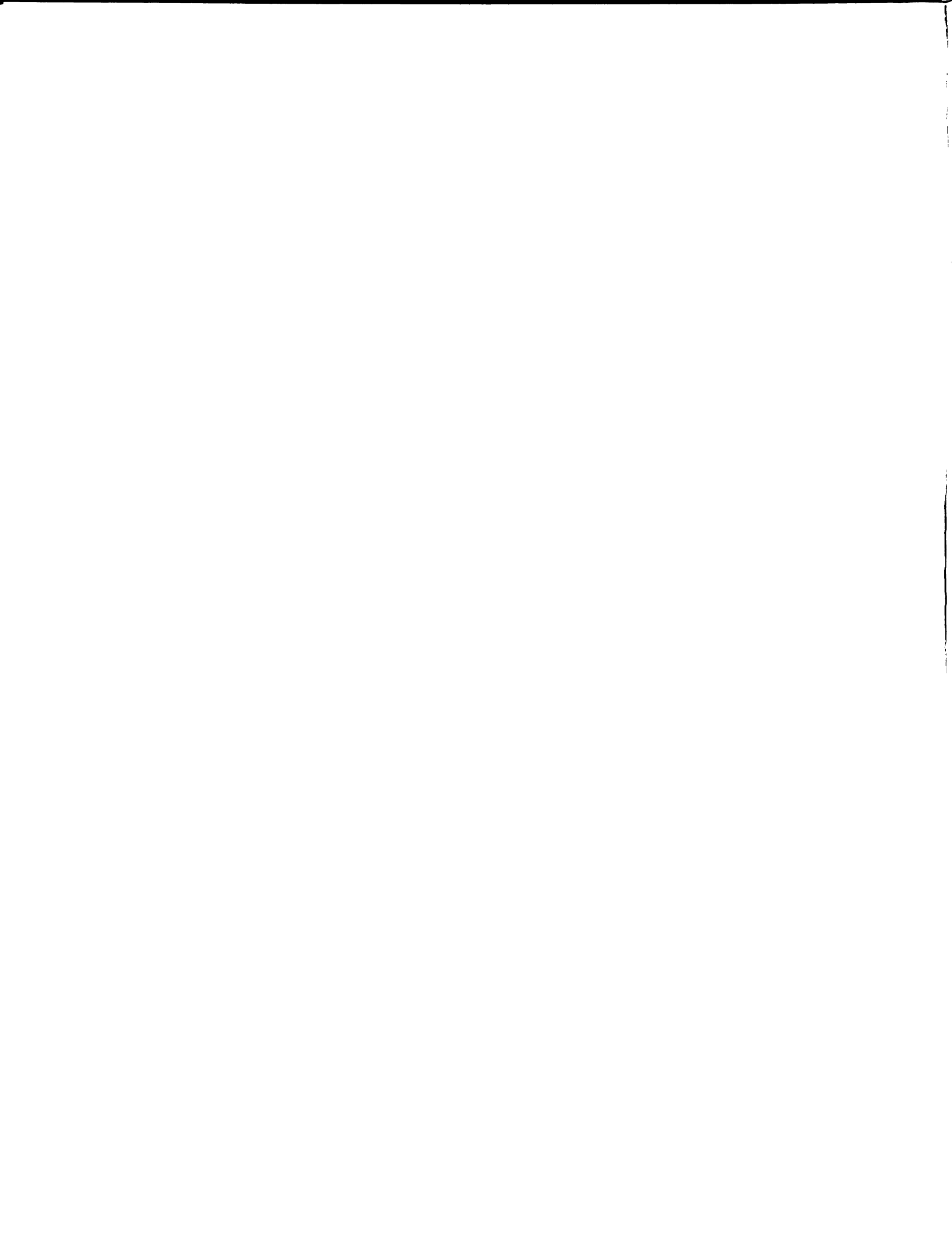
or
$$\text{Cosh } mx (2 \text{Cosh } mp - 2 - \omega^2) = 0$$

Since $\text{Cosh } mx \neq 0$, one obtains

$$2 \text{Cosh } mp - 2 - \omega^2 = 0$$

or
$$mp = \text{Cosh}^{-1} \frac{\omega^2 + 2}{2}$$

or
$$m = (1/p) \text{Cosh}^{-1} \frac{(\omega^2 + 2)}{2} \quad (1.8)$$



Therefore,

$F = A \text{ Cosh } mx$, where m is given by Eq. (1.8), is a solution of the difference Eq. (1.6). In a similar manner one can show that

$F = B \text{ Sinh } mx$, is also a solution of Eq. (1.6). Thus, the general solution of Eq. (1.6) is a linear combination of above two solutions, i. e.,

$$F_c = A \text{ Cosh } mx + B \text{ Sinh } mx \quad (1.9)$$

To obtain the particular solution of Eq. (1.5) an analogy with differential equations is again made, in which case, one proceeds as follows:

Let

$$F_p = a, \text{ a constant}$$

Thus $\Delta^2 F_p = 0$

Substituting this value of $\Delta^2 F$ in Eq. (1.5) yields

$$-\omega^2 F_p = -P\omega_1^2$$

or $F_p = (\omega_1^2/\omega^2)P \quad (1.10)$

Therefore, the final solution of the difference equation (1.5) becomes

$$\begin{aligned} F &= F_c + F_p \\ &= A \text{ Cosh } mx + B \text{ Sinh } mx + (\omega_1^2/\omega^2)P \end{aligned} \quad (1.11)$$

where A and B are to be obtained from the boundary conditions.

The boundary conditions are

1. $F = 0$ at $x = 0$
2. $F = P$ at $x = np$, where $n =$ total number of connectors.

Using the first boundary condition one obtains

$$0 = A + (\omega_1^2/\omega^2)P$$

$$\text{or } A = (-\omega_1^2/\omega^2)P \quad (1.12)$$

and the second boundary condition gives

$$P = A \text{ Cosh } m np + B \text{ Sinh } m np + (\omega_1^2/\omega^2)P$$

$$\text{or } B = [P - A \text{ Cosh } m np - \omega_1^2/\omega^2 P] / [\text{Sinh } m np] \quad (1.13)$$

Analysis by the Principle of Minimum Complementary Energy

The analysis presented here utilizes the principle of minimum complementary energy. This principle can be stated as follows:

when true state of stress is varied by an infinitesimal amount in a system in such a manner that the new state again constitutes equilibrium with the given set of external loads, the first order change in the complementary energy less the work done by the increments of the reactions while traveling through the actual displacements of the supports is equal to zero. Or, mathematically

$$\delta U' - \sum r_n \delta R_n = 0$$

where

$\delta U'$ = the first variation in the complementary energy

r_n = displacement of the n th reaction

δR_n = the first variation in the n th reaction.

In applying this principle to the metal plate connected timber joint, the following assumptions were made:

1. The metal plate connectors instead of being driven into the wood are glued to the wood surface by a fictitious adhesive of negligible thickness, thus, forming a continuous contact between the metal plate and the wood.
2. The wood consists of two parts; one concentrated mass that takes all the normal stresses while the second thin part takes the shearing stress alone.
3. The joint behaves as a linearly elastic material.

Since the joint is symmetrical about the middle, only one-half portion is necessary for analysis. This part of the joint is shown in Figure 3.

Considering equilibrium of an element dx across the joint, one obtains the state of stress as shown in Figures 4a, b and c.

From Figure 4b, considering the equilibrium of forces in the x-direction one obtains,

$$\left(\tau + \frac{\partial \tau}{\partial y} dy \right) t dx - \tau t dx = 0 \quad (2.1)$$

or $\frac{\partial \tau}{\partial y} = 0$ which implies that τ is independent of y .

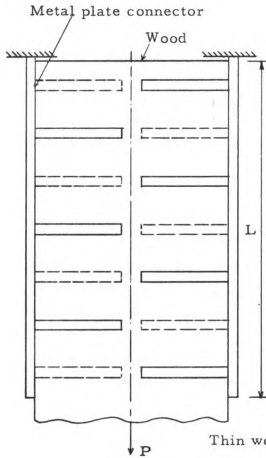
From Figure 4a, considering the equilibrium of forces in the x-direction one obtains

$$\frac{d\sigma_c}{dx} dx A_c + \tau t dx = 0$$

or $\frac{d\sigma_c}{dx} + \frac{t}{A_c} \tau = 0 \quad (2.2)$

$$\text{or } \sigma_c \int_0^x = - \frac{t}{A_c} \int_0^x \tau dx$$

ACTUAL JOINT



IDEALIZED JOINT

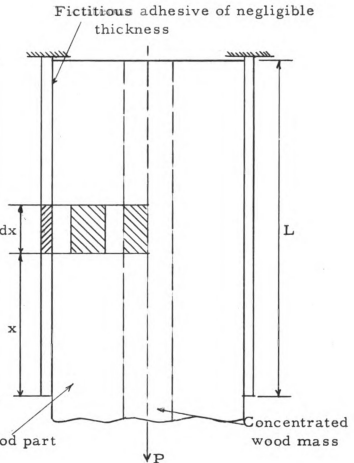


Fig. 3. Actual and idealized joints used in the analysis.

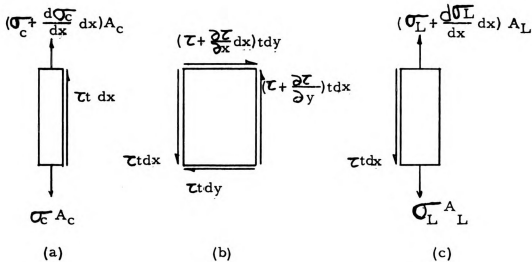


Fig. 4. Equilibrium of small elements across the idealized joint.

But σ_c vanishes at $x = 0$

therefore,

$$\sigma_c = -\frac{t}{A_c} \int_0^x \tau \, dx \quad (2.3)$$

From Figure 4c, considering the equilibrium of forces in the x-direction one obtains

$$\frac{d\sigma_L}{dx} \, dx \, A_L - \tau t \, dx = 0$$

$$\text{or} \quad \frac{d\sigma_L}{dx} - \frac{\tau t}{A_L} = 0 \quad (2.4)$$

$$\text{or} \quad \sigma_L \Big|_0^x = \int_0^x \frac{\tau t}{A_L} \, dx$$

$$\text{But} \quad \sigma_L = \frac{P}{2A_L} \text{ at } x = 0$$

hence

$$\sigma_L = \frac{P}{2A_L} + \frac{t}{A_L} \int_0^x \tau \, dx \quad (2.5)$$

Replacing τ by $-\frac{d\sigma_c}{dx} \frac{A_c}{t}$ from Eq. (2.2), Eq. (2.5) becomes

$$\sigma_L = \frac{P}{2A_L} - \frac{A_c}{A_L} (\sigma_c)$$

as

$$\sigma_c = 0 \text{ at } x = 0$$

Derivation of Differential Equation

The total strain energy of the joint can be written as

$$U_T = U_\tau + U_{\sigma_L} + U_{\sigma_c} \quad (2.6)$$

where

U_{τ} = strain energy due to shearing stress τ and

so on.

$$\begin{aligned} U_{\tau} &= 2 \left[\int_v \frac{\tau^2}{2G} dv \right] \\ &= \frac{bt}{G} \int_0^L \left(\frac{A_c}{t} \right) \left(\frac{d\sigma_c}{dx} \right)^2 dx \end{aligned} \quad (2.6a)$$

$$\begin{aligned} U_{\sigma_L} &= 2 \left[\int_v \frac{\sigma_L^2}{2E_L} dv \right] \\ &= \frac{A_L}{E_L} \int_0^L \left(\frac{P}{2A_L} - \frac{A_c}{A_L} \sigma_c \right)^2 dx \end{aligned} \quad (2.6b)$$

and

$$\begin{aligned} U_{\sigma_c} &= 2 \left[\int_v \frac{\sigma_c^2}{2E_c} dv \right] \\ &= \frac{A_c}{E_c} \int_0^L \sigma_c^2 dx \end{aligned} \quad (2.6c)$$

A change δU_T in the total strain energy corresponding to a change in the stress σ_c by $\delta \sigma_c$ can be expressed as

$$\delta U_T = \delta U_{\tau} + \delta U_{\sigma_L} + \delta U_{\sigma_c} \quad (2.7)$$

The individual variations can be evaluated as follows, if terms involving squares and products of the infinitesimal variations and of their derivatives are neglected.

$$\begin{aligned} \delta U_{\tau} &= \frac{bt}{G} \left(\frac{A_c}{t} \right)^2 \int_0^L \left[\left(\frac{d\sigma_c + \delta\sigma_c}{dx} \right)^2 - \left(\frac{d\sigma_c}{dx} \right)^2 \right] dx \\ &= \frac{bt}{G} \left(\frac{A_c}{t} \right)^2 \int_0^L \left[\cancel{\left(\frac{d\sigma_c}{dx} \right)^2} + \cancel{\left(\frac{d\delta\sigma_c}{dx} \right)^2} + 2 \frac{d\sigma_c}{dx} \frac{d\delta\sigma_c}{dx} - \cancel{\left(\frac{d\sigma_c}{dx} \right)^2} \right] dx \\ &= \frac{bt}{G} \left(\frac{A_c}{t} \right)^2 \int_0^L 2 \frac{d\sigma_c}{dx} \frac{d\delta\sigma_c}{dx} dx \end{aligned} \quad (2.7a)$$

In a similar manner

$$\delta U_{\sigma_L} = 2 \frac{A_L}{E_L} \int_0^L \left(\frac{A_c}{A_L} \sigma_c - \frac{P}{2A_L} \right) \delta \sigma_c \, dx \quad (2.7b)$$

and

$$\delta U_{\sigma_c} = 2 \frac{A_c}{E_c} \int_0^L \sigma_c \delta \sigma_c \, dx \quad (2.7c)$$

Now in order to eliminate $\frac{d\delta\sigma_c}{dx}$ from Eq. (2.7a), the use of integration by parts is made, i. e.,

$$\int_0^L \frac{d\sigma_c}{dx} \frac{d\delta\sigma_c}{dx} \, dx = uv \Big|_0^L - \int_0^L v \, du$$

$$\text{where } u = \frac{d\sigma_c}{dx}, \quad dv = \frac{d\delta\sigma_c}{dx},$$

$$= \frac{d\sigma_c}{dx} \delta\sigma_c \Big|_0^L - \int_0^L \frac{d^2\sigma_c}{dx^2} \delta\sigma_c \, dx$$

but $\delta\sigma_c = 0$ at $x = 0$ and $x = L$ because both the actual and the varied stress states must be in equilibrium with the applied loads there.

Therefore,

$$\int_0^L \frac{d\sigma_c}{dx} \frac{d\delta\sigma_c}{dx} \, dx = - \int_0^L \frac{d^2\sigma_c}{dx^2} \delta\sigma_c \, dx$$

Thus

$$\begin{aligned} \delta U_T &= -2 \frac{bA_c^2}{Gt} \int_0^L \frac{d^2\sigma_c}{dx^2} \delta\sigma_c \, dx \\ &+ 2 \frac{A_L}{E_L} \int_0^L \left(\frac{A_c}{A_L} \sigma_c - \frac{P}{2A_L} \right) \delta\sigma_c \, dx \\ &+ 2 \frac{A_c}{E_c} \int_0^L \sigma_c \delta\sigma_c \, dx \end{aligned}$$

$$\begin{aligned}
&= \int_0^L \left[-2 \frac{bA_c^2}{Gt} \frac{d^2 \sigma_c}{dx^2} + \frac{2A_c}{E_L} \left(\frac{A_c \sigma_c}{A_L} - \frac{P}{2A_L} \right) \right. \\
&\quad \left. + 2 \frac{A_c}{E_c} \sigma_c \right] \delta \sigma_c dx \quad (2.8)
\end{aligned}$$

Now making use of the principle of minimum complementary energy which states that

$\delta (U' + V') = 0$ for equilibrium, and noting that $\delta V' = 0$, as the reactions are unyielding, and $U' = U$, as the materials are assumed to be linearly elastic, one obtains

$$\delta U = 0$$

Therefore, for any arbitrary variation $\delta \sigma_c$ it must be that

$$\begin{aligned}
&- 2 \frac{bA_c^2}{Gt} \frac{d^2 \sigma_c}{dx^2} + 2 \frac{A_c}{E_L A_L} \left(A_c \sigma_c - \frac{P}{2} \right) + 2 \frac{A_c}{E_c} \sigma_c = 0 \\
\text{or } &\frac{d^2 \sigma_c}{dx^2} - k^2 \sigma_c = - \frac{Gt}{2bE_L A_c A_L} P \quad (2.9)
\end{aligned}$$

$$\text{where } k^2 = \left(\frac{1}{E_L A_L} + \frac{1}{E_c A_c} \right) \frac{Gt}{b}$$

Solution of Differential Equation (2.9)

The differential equation (2.9) can be solved by well-known methods of ordinary linear differential equation theory. The solution can be written in two parts: σ_c /complementary and σ_c /particular.

Then

$$\begin{aligned}
\sigma_c &= \sigma_c/\text{complementary} + \sigma_c/\text{particular} \\
\sigma_c/\text{complementary} &= A \cosh kx + B \sinh kx \\
\sigma_c/\text{particular} &= + \frac{E_c}{2(A_L E_L + A_c E_c)}
\end{aligned}$$

Therefore,

$$\sigma_c = A \cosh kx + B \sinh kx + \frac{E_c}{2(A_L E_L + A_c E_c)}$$

where A and B are constants of integration and are determined from the following two boundary conditions

1. $\sigma_c = 0$ at $x = 0$
2. $\sigma_c = \frac{P}{2A_c}$ at $x = L$

From the first boundary condition:

$$0 = A + \frac{E_c}{2(E_L A_L + E_c A_c)} P$$

Therefore

$$A = - \frac{E_c}{2(E_L A_L + E_c A_c)} P \quad (2.10)$$

From the second boundary condition

$$B = \frac{1}{\sinh kL} \left[\frac{P}{2A_c} + \frac{E_c}{2(E_L A_L + E_c A_c)} (\cosh kL - 1) \right]$$

Finally

$$\begin{aligned} \sigma_c = \frac{P}{2} & \left[- \frac{E_c}{E_T A_T} \cosh kx + \frac{\sinh kx}{\sinh kL} \left\{ \frac{1}{A_c} + \frac{E_c}{E_T A_T} (\cosh kL - 1) \right\} \right. \\ & \left. + \frac{E_c}{E_T A_T} \right] \end{aligned}$$

where $(A_L E_L + A_c E_c) = A_T E_T$

EXPERIMENTAL INVESTIGATION

Two techniques of experimental stress analysis; namely, PhotoStress^{*} and a strain gage technique were used to determine the stress distribution in the metal plate. The PhotoStress analysis was used to obtain an overall picture of stress distribution in the entire plate while strain gages were used to give accurate and reliable strain measurements at a network of points.

PhotoStress Analysis

The PhotoStress technique of stress analysis has been extensively used in the past few years to determine the surface strains on metals as well as non-metallic surfaces. It has also been demonstrated by Agostino et al. (1955) that this technique yields a good measure of interface strains for both elastic and plastic deformation of the metal part.

The PhotoStress technique employs the birefringent properties exhibited by certain materials when strained. This birefringence is directly proportional to the intensity of strain. The surface to be stress analyzed is coated with a special transparent plastic. The birefringence is observed and measured with polarized light in a specially designed instrument called a reflection polariscope.

An important advantage of this technique over other means of strain measurement is that the strain is obtained over the entire coated area simultaneously.

* Trade name for birefringent coating.

Test Specimen

The test specimen consisted of two pieces of nominal 2" x 4" structural grade Douglas fir, butted together, and fastened by two 16-gauge, $2\frac{7}{8}$ " x $7\frac{7}{8}$ " metal plate connectors, one on each face of the joint. The shape of the teeth punched in the plate is shown in Figure 5. The overall length of the test specimen was 26". The details of specimen are shown in Figure 6. The joint was made in the laboratory by pressing the teeth in with a hydraulic press.

Two PhotoStress sheet plastics (sheet type S, K factor 0.083 and thickness $.121 \pm .002$ in.) of approximately the same size as the metal plate were bonded with reflective cement onto each of the plates. The outer surfaces of the metal plates had been sandblasted before they were attached to the wood. Sandblasting was found necessary to allow the cement to transmit the surface strains from the plate to the plastic. This fact was revealed by a test made on a specimen bonded with a clear cement on an aluminum painted surface. Reflective cement was used to give a better reflecting surface and hence a clear fringe pattern. The effect of sand blasted surface with reflective cement was remarkably good in revealing the necessary details of isochromatics and isoclinics.

The PhotoStress plastic was made in approximately the same shape as the plate with punched holes similarly located. Considerable difficulty was encountered in making the intricate holes precisely. It was found in preliminary trials that the plastics must be made to conform to the shape of the specimen precisely for accurate measurements.

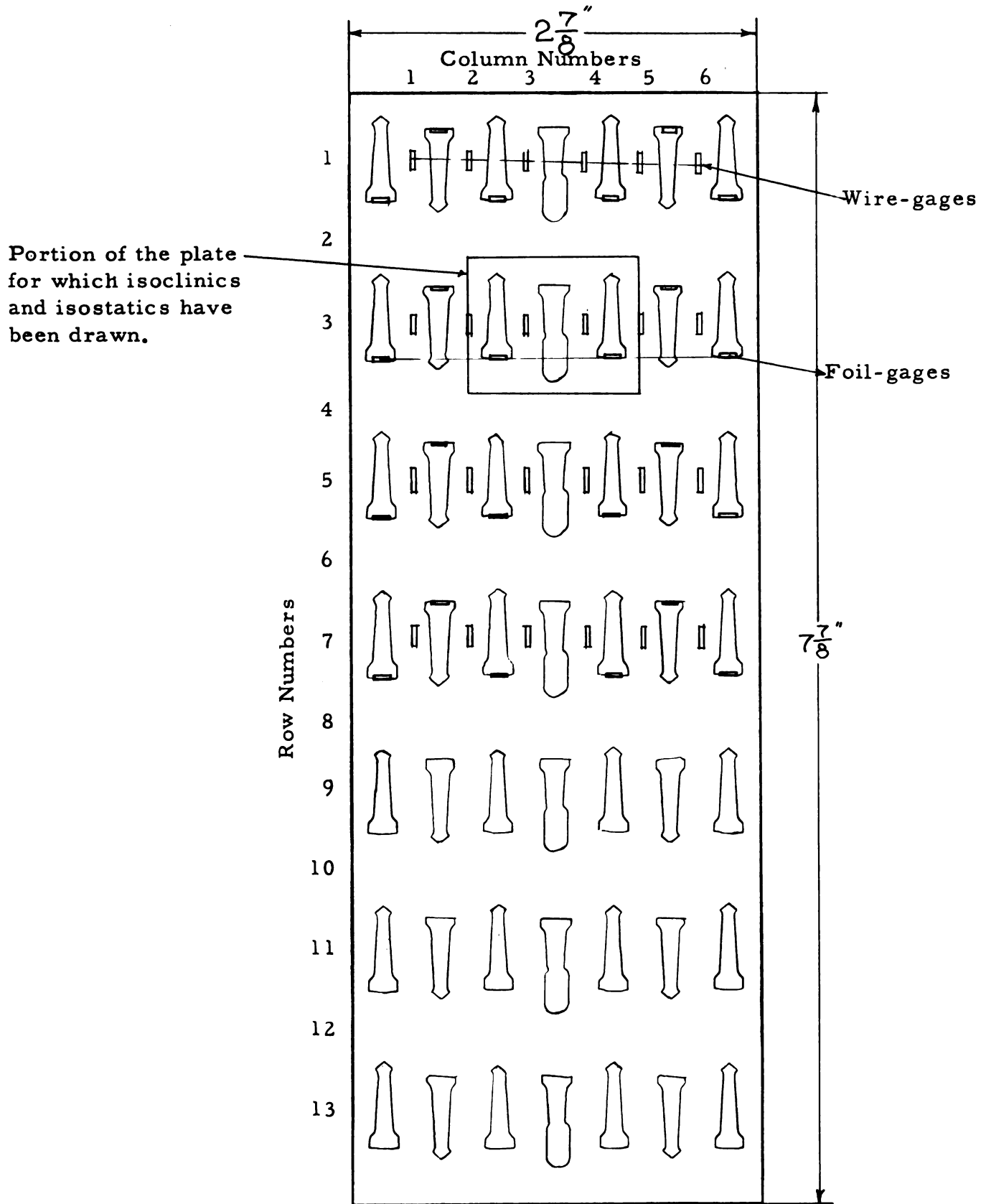


Fig. 5. Shape of the punched teeth in the metal plate connector and location of strain gages.

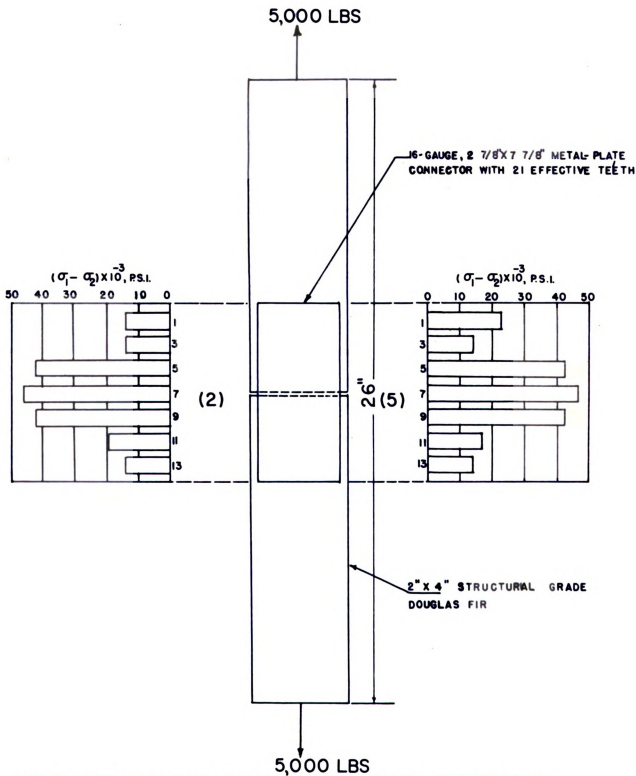


FIG. 6 TEST SPECIMEN AND PRINCIPAL STRESS DIFFERENCE VARIATION ALONG COLUMNS 2 AND 5

Testing Procedure

The specimen was mounted in a Baldwin testing machine and loaded in uniaxial tension. Figure 7 shows the equipment used for testing. The load was applied in increments of 500 lbs. The isochromatic (locus of points with constant principal stress difference) patterns were observed through a large field PhotoStress meter as loading proceeded. The loading was continued until good isochromatic patterns were observed, which was around 5000 lbs. (approximately 5/8 of the ultimate load).

The data were taken photographically. Six isochromatic pictures, with α (angular parameter of analyzer) ranging from 0 to 75° were taken at intervals of 15°. To obtain a good isoclinic (locus of points with same principal stress directions) pattern, nine isoclinic pictures with parameters ranging from 0 to 80° were taken at intervals of 10°.

The PhotoStress meter was placed at a distance of 5 feet from the specimen. Ektachrome, type-B, high-speed film was used in a 35 mm camera. The shutter was opened for 1/11 seconds at an f 22 lens opening. A 135 mm telephoto lens was used. The photographs thus obtained gave the necessary detail.

A point by point measurement of isochromatic fringe order was also made at a network of 78 points on the plate.

The data from the photographs were transferred onto sheets of paper by tracing fringe as well as isoclinic patterns.

Results and Discussion of PhotoStress Analysis

Stress Magnitudes

The results of stress distribution at a finite network of points as determined by the PhotoStress Analysis are given in Table I. The location and numbering system of the points is shown in Figure 5.

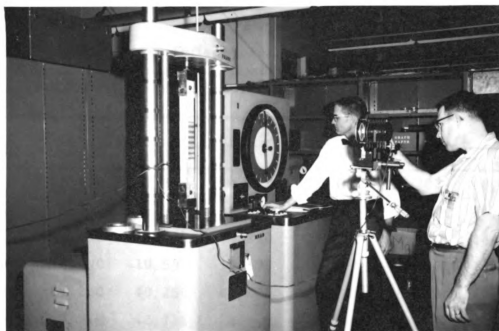


Fig. 7. Test apparatus for PhotoStress study.

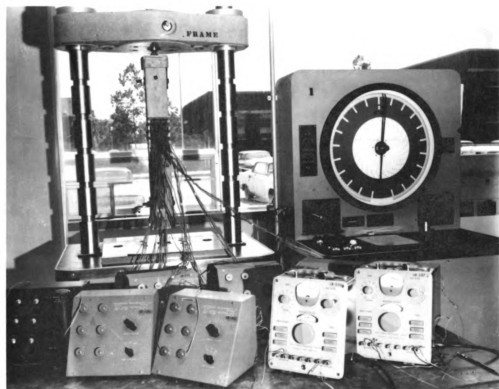


Fig. 8. Test apparatus for strain gage investigation.

Table I. Principal Stress Differences at a Network of Points in the Metal Plate Connector, Loaded in Tension. (System of Point Designation is Shown in Figure 5)

Rows	Columns					
	1	2	3	4	5	6
1	16,900	14,810	14,810	14,810	23,202	16,900
2	16,900	16,900	-6,350	-6,350	16,900	16,900
3	14,810	14,810	14,810	14,810	14,810	14,810
4	-10,590	-10,590	-10,590	-10,590	-10,590	-10,590
5	40,250	40,250	40,250	40,250	40,250	40,250
6	-2,118	-2,118	-2,118	-2,118	-2,118	-2,118
7	46,500	46,500	46,500	46,500	46,500	46,500
8	-2,118	-2,118	-2,118	-2,118	-2,118	-2,118
9	40,250	40,250	40,250	40,250	40,250	40,250
10	16,900	-10,590	-10,590	-10,590	-10,590	16,900
11	16,325	19,000	19,000	19,000	16,650	14,620
12	16,900	-8,490	-8,490	-8,490	-8,490	16,900
13	14,810	14,810	14,810	14,810	14,810	14,810

This table was prepared using photographic as well as point by point measurement data. The following equation as given by Zandman (1959) in his booklet Photostress--Principles and Applications, was used to calculate the principal stress differences.

$$(\sigma_1 - \sigma_2) = \delta \frac{E}{1 + \mu}$$

where $\delta = n\lambda \pm \frac{\alpha\lambda}{180}$ = relative retardation

n = the fringe order

α = angular parameter of analyzer

λ = wave length of the monochromatic light =
 2.27×10^{-5} in.

E = Modulus of elasticity of steel =
 30×10^6 psi.

μ = Poisson's ratio for steel = 0.25

t = thickness of plastic = 0.1195 in.

k = strain optical coefficient of the plastic =
 0.09.

Thus substituting in the known values,

$$(\sigma_1 - \sigma_2) = 1119.9 \times 10^6 \delta \text{ psi.}$$

The principal stress differences are plotted in Figures 9, 10 and 11 at the network of selected points. For direct comparison, $(\sigma_1 - \sigma_2)$ are also plotted in Figure 6 along the plate length. From Table I and Figures 9, 10 and 11, it is clear that principal stress differences are nearly symmetrical about the axis of loading and normal to it. The variation of $(\sigma_1 - \sigma_2)$ in the transverse direction is negligible. This indicates that there was no appreciable eccentricity in loading. The principal stress differences at the central strips are maximums and decrease rather rapidly towards each end along the axis of loading. The maximum stress difference was 46,500 psi at the central strips while minimum was 14,810 psi closer to the ends.

The stresses at the central strips along row 7 were calculated by dividing the total axial load on one plate by the effective cross-sectional area of the plate. In Table II these stresses are compared with the measured stresses. It is clear from this table that measured stresses are influenced by slight variation in the E and μ combination. The percent difference between measured and calculated values ranged from 9.61 to 42.2% assuming that the measured values were correct.

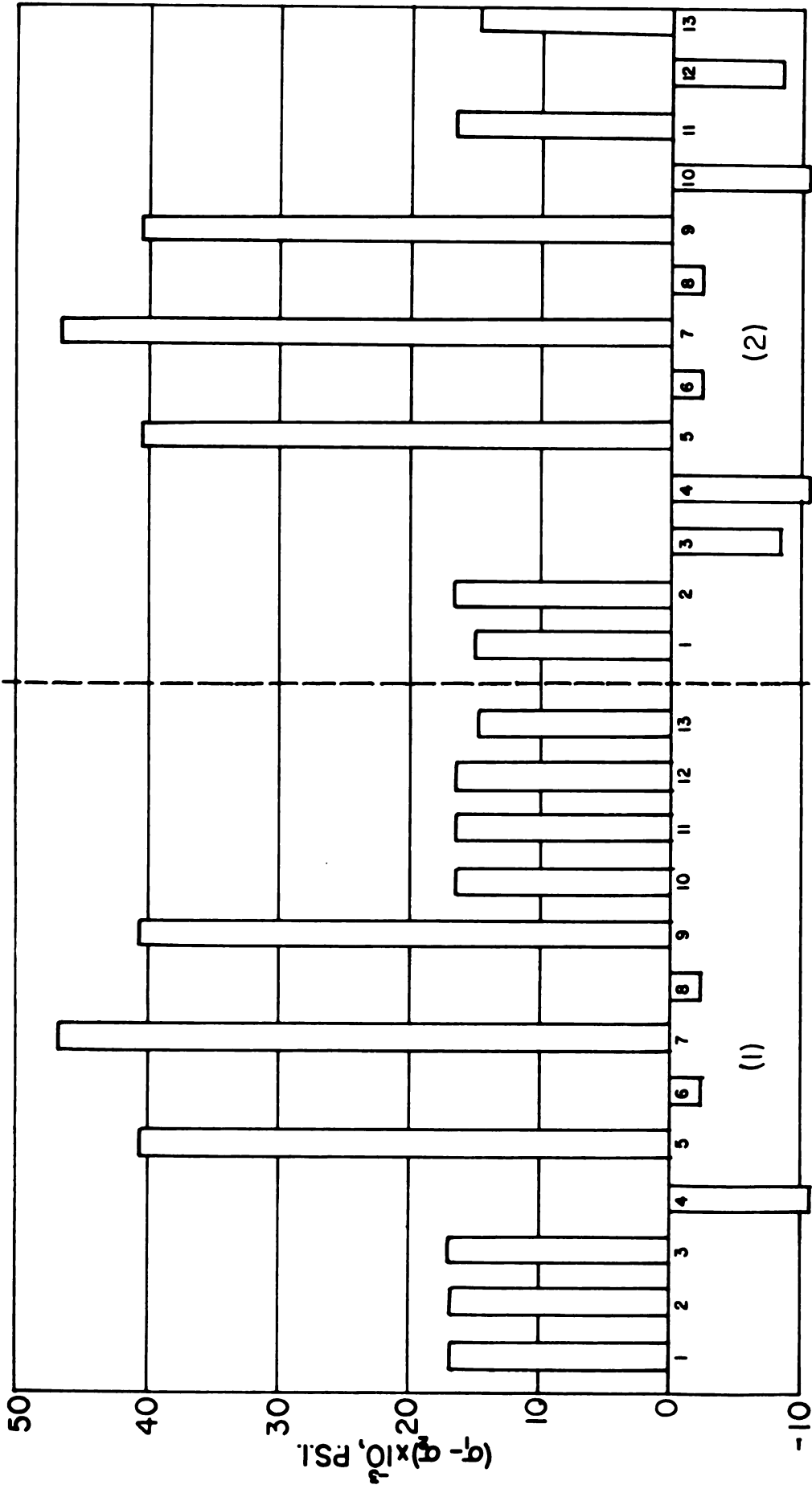
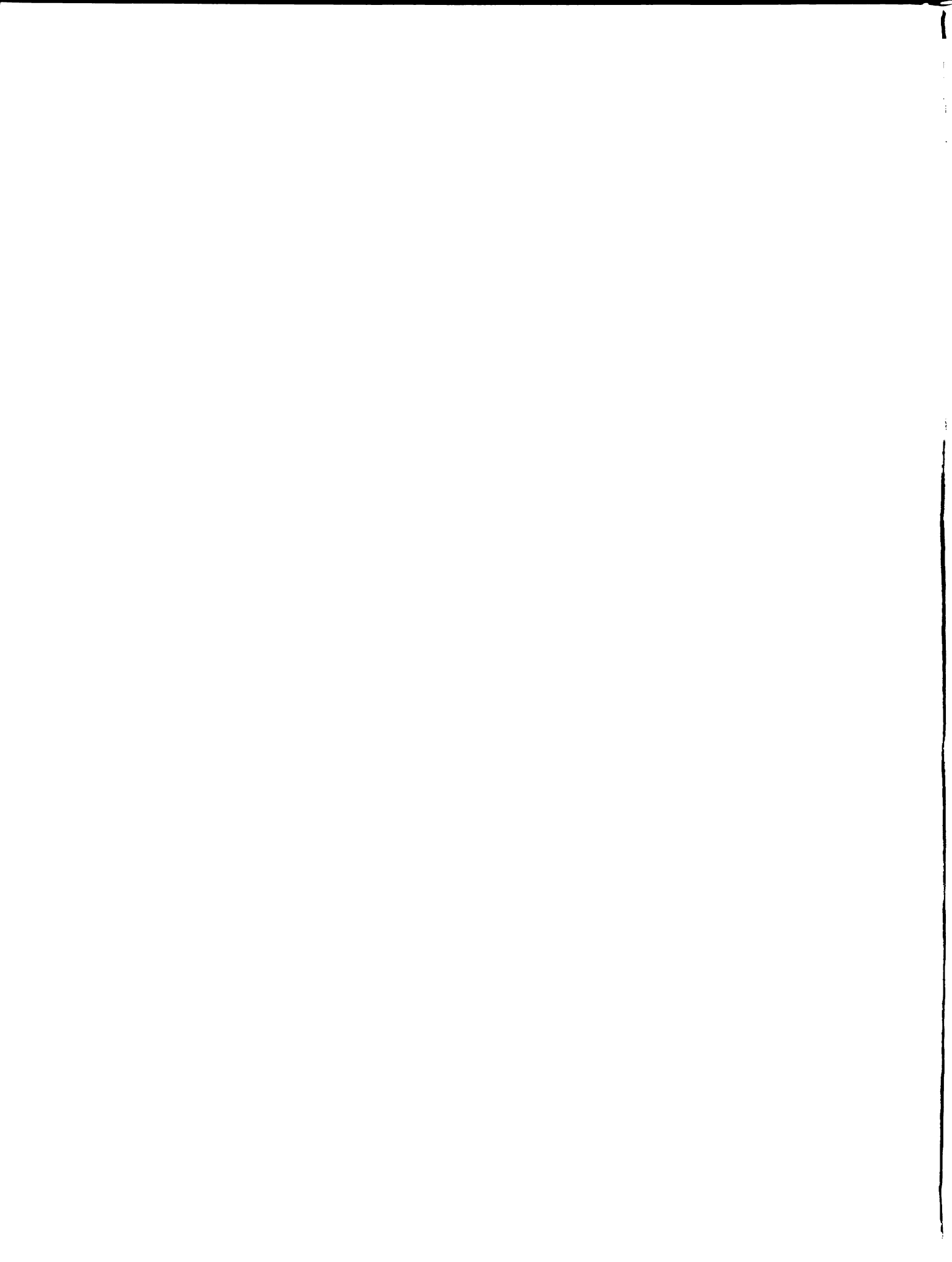


FIG. 9 HISTOGRAM REPRESENTATION OF PRINCIPAL STRESS DIFFERENCES ALONG COLUMNS 1 AND 2



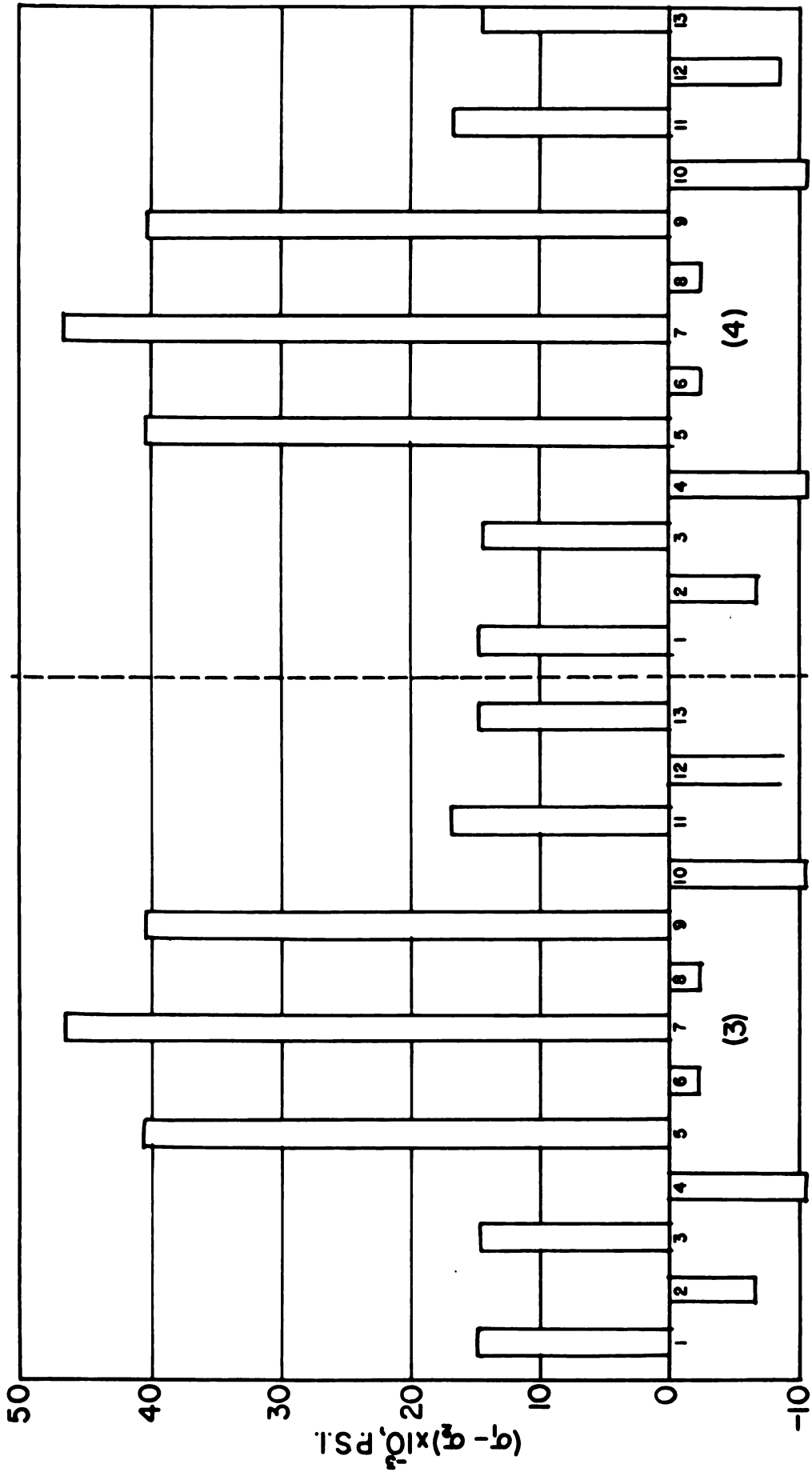


FIG. 10 HISTOGRAM REPRESENTATION OF PRINCIPAL STRESS DIFFERENCES ALONG COLUMNS 3 AND 4

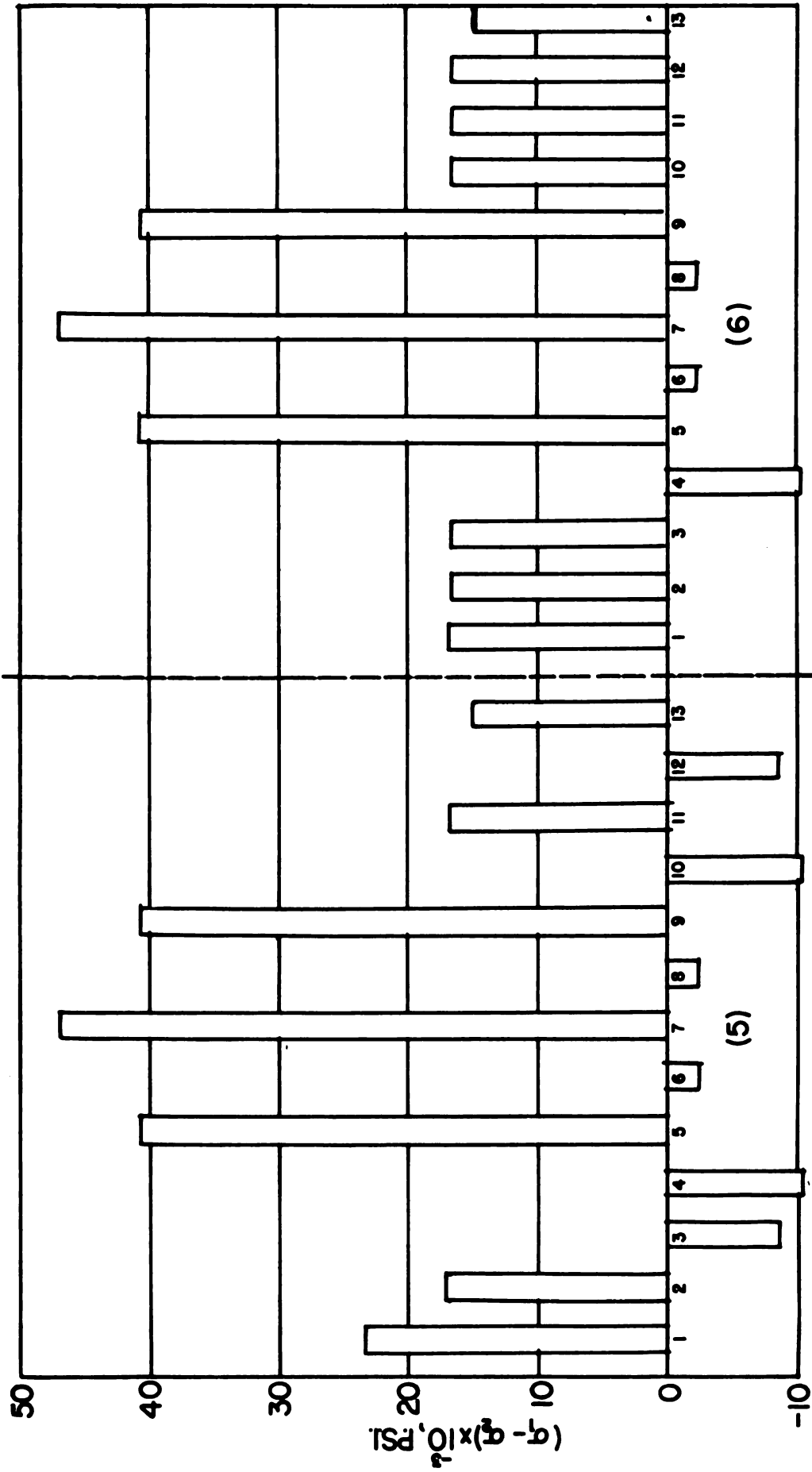


FIG. 11 HISTOGRAM REPRESENTATION OF PRINCIPAL STRESS DIFFERENCES ALONG COLUMNS 5 AND 6

Table II. Comparison of Measured and Calculated Stresses on Strips Along Row 7 at a Uniaxial Tensile Load of 2500 Lbs Per Plate

E psi x 10 ⁻⁶	μ	Calculated Stress psi	Measured Stress psi	% Diff.
30	.25	26,100	37,200	42.2
30	.30	26,100	34,300	31.4
29	.30	26,100	33,200	27.2
29	.35	26,100	30,800	18.0
29	.4	26,100	28,610	9.61

These large differences may be due partly to the E and μ effect and due partly to the strain gradient effect mentioned by Duffy (1961) as this was prevalent in this case. Furthermore, the effect of stress concentrations around the holes may be another contributing factor.

Stress Directions

Isoclinics. A set of isoclinics are drawn in Figure 12 for a portion of the plate. The location of this portion of the plate is shown in Figure 5. These isoclinics were drawn from the superposition of the tracings of the isoclinic photographs. Each isoclinic was represented by a best line through its black portion. Smooth curves, with some corrections, were drawn after the whole field was completed.

It should be noted here that there are ten isotropic points in this portion of the plate. Complete isoclinic patterns around three of them are shown.

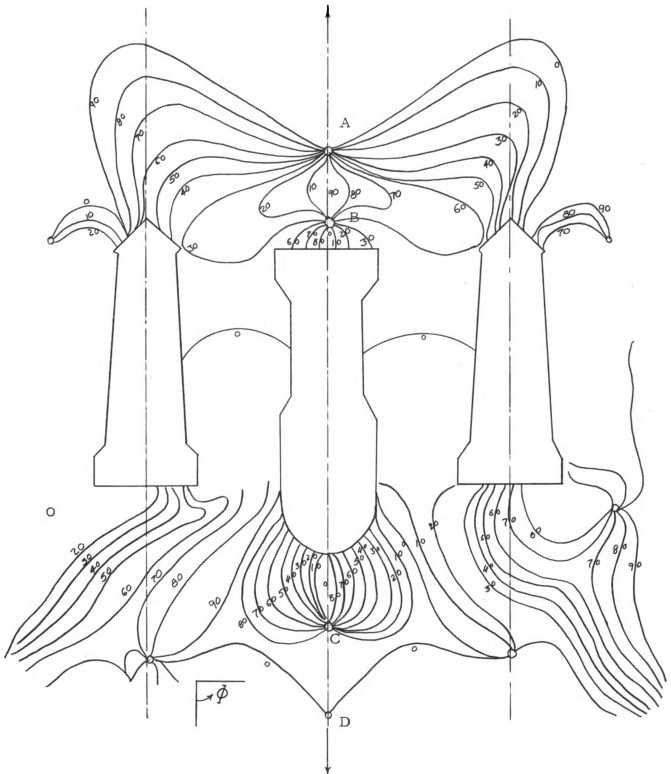


Fig. 12. Isoclinics in a metal plate connector, loaded in uniaxial tension. (The location of this portion on the plate is shown in Fig. 5.)

An isotropic point is defined as a point at which the two principal stresses are equal. At such points, the state of stress is therefore hydrostatic and isoclinics of different parameters can intersect each other. Shear stresses, of course, are zero at these points and hence every direction is a principal direction.

Referring to Figure 12, point A is a negative isotropic point while B and C are positive as the isoclinic parameters around these points increase in the counterclockwise direction. Two neighboring isotropic points must be of opposite sign, as they are in the upper portion, and therefore point D must also be a negative isotropic point.

As is evident from the figure, the isoclinics are very nearly symmetrical about the axis of loading.

Stress Trajectories (Isostatics). Stress trajectories for the portion of the plate already mentioned are shown in Figure 13. These are orthogonal curves representing the principal stress directions at every point through which they pass. This drawing was made from the isoclinic diagram using the method discussed by Hetenyi (1950).

It is clear from Figure 13 that stress directions at the middle of unpunched strips are very nearly in the direction of loading and normal to it. However, these directions change some distance away from the middle. This is due to stress concentrations around intricate shapes of the punched portion in this multiconnected body.

The stress trajectories around the isotropic points should be particularly noted. Although stress trajectories around only three of the isotropic points are shown, nevertheless, they illustrate all the principal types of isostatics. The stress trajectories around the uppermost point A are of the asymptotic or non-interlocking type and are negative. Those around point B are of the interlocking type and are

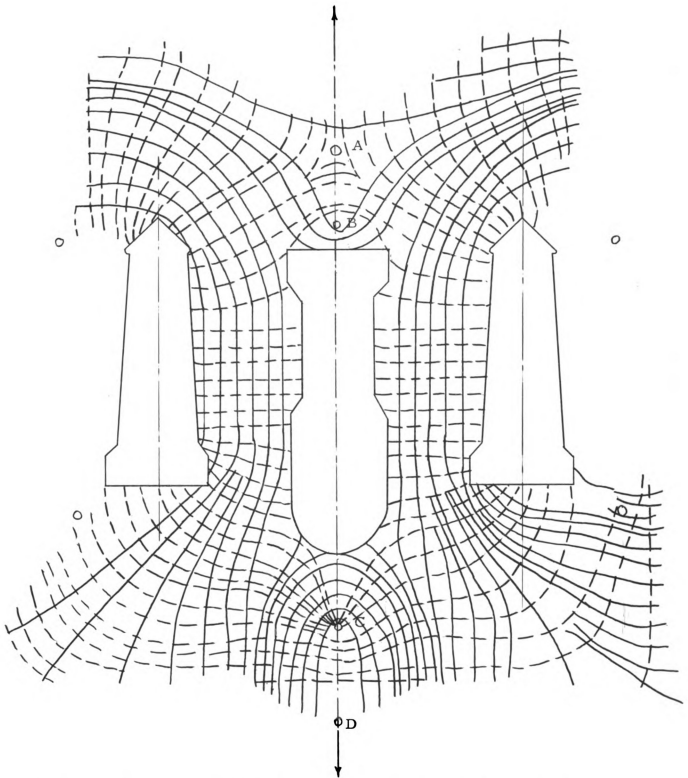


Fig. 13. Stress trajectories in a metal plate connector, loaded in uniaxial tension.

positive. The stress trajectories around point C are of the mixed type. They are positive since the isoclinic parameter increases in the counterclockwise direction.

From the preceding discussion of the PhotoStress analysis, it is evident that the stresses and their directions in the metal plate are rather complicated. The stress trajectories shown in Figure 13 indicate that the principal stress direction in the middle of the flat strips was in the direction of loading and normal to it. This fact was later utilized in bonding the strain gages to these strips for accurate and reliable measurement of the principal stress.

Strain Gage Analysis

The stresses in the metal plate at a network of 48 points were determined from strain measurements with SR-4 strain gages. The location of these gages on the plate is shown in Figure 5. Twenty-four of these gages, bonded on the flat strips, were A-18 wire-type with gage factor of 1.79. These wire gages had a nominal gage length of $1/8$ inch. The other twenty-four were of the FAP-6 foil-type with a gage factor of 1.99. The foil-type gages had a nominal gage length of $1/16$ inch and were bonded to the bases of the miniature cantilever teeth.

Test Specimen

The test specimen was similar to the one used for PhotoStress analysis. It consisted of two pieces of nominal 2" x 4" structural grade Douglas fir held together by two $2\frac{7}{8}$ " x $7\frac{7}{8}$ " 16-gauge metal plates, one on each face of the joint. The joint was made in the laboratory using a hydraulic press. The metal plates were sandblasted before being fastened to the wood. The strain gages were bonded with Eastman 910 contact cement.

Testing Procedure

The test specimen was mounted in a Baldwin testing machine and loaded in tension. Figure 8 shows the joint in testing position. Multiple switching units and strain indicators are also shown.

The load was applied gradually in increments of 500 pounds to a maximum of 5,000 pounds. (In the last test only, the joint was loaded to 7,000 pounds.) The readings were taken manually at each interval of 500 pounds. Two persons required approximately five minutes to complete the reading of 48 gages. The load during this period was held constant.

Two sets of readings were taken to insure the accuracy of the data. Stresses were calculated from the measured strains. The modulus of elasticity used for steel was 30×10^6 psi. The stresses thus calculated were plotted and results compared.

Results and Discussion of Strain Gage Analysis

Figures 14, 15, 16, 17, 18 and 19 show the load stress curves as obtained from wire-type gages mounted on the flat strips of the plate. It is clear from these curves that the load stress relations are fairly linear up to 5,000 lbs axial load. The stress in one extreme column one was higher than the opposite column six and thereby indicating the existence of slight eccentricity. It is also apparent from these curves that the second set of gages in row five were indicating the highest stress and not the middle one (row seven) as one would guess. It was further observed that as the load was increased to 7,000 lbs, the highest stress, instead of occurring along row five, occurred in the middle of the joint.

The results of the tension test for a single load of 5,000 lbs are shown in Figures 20 and 21. For brevity the results of only one test

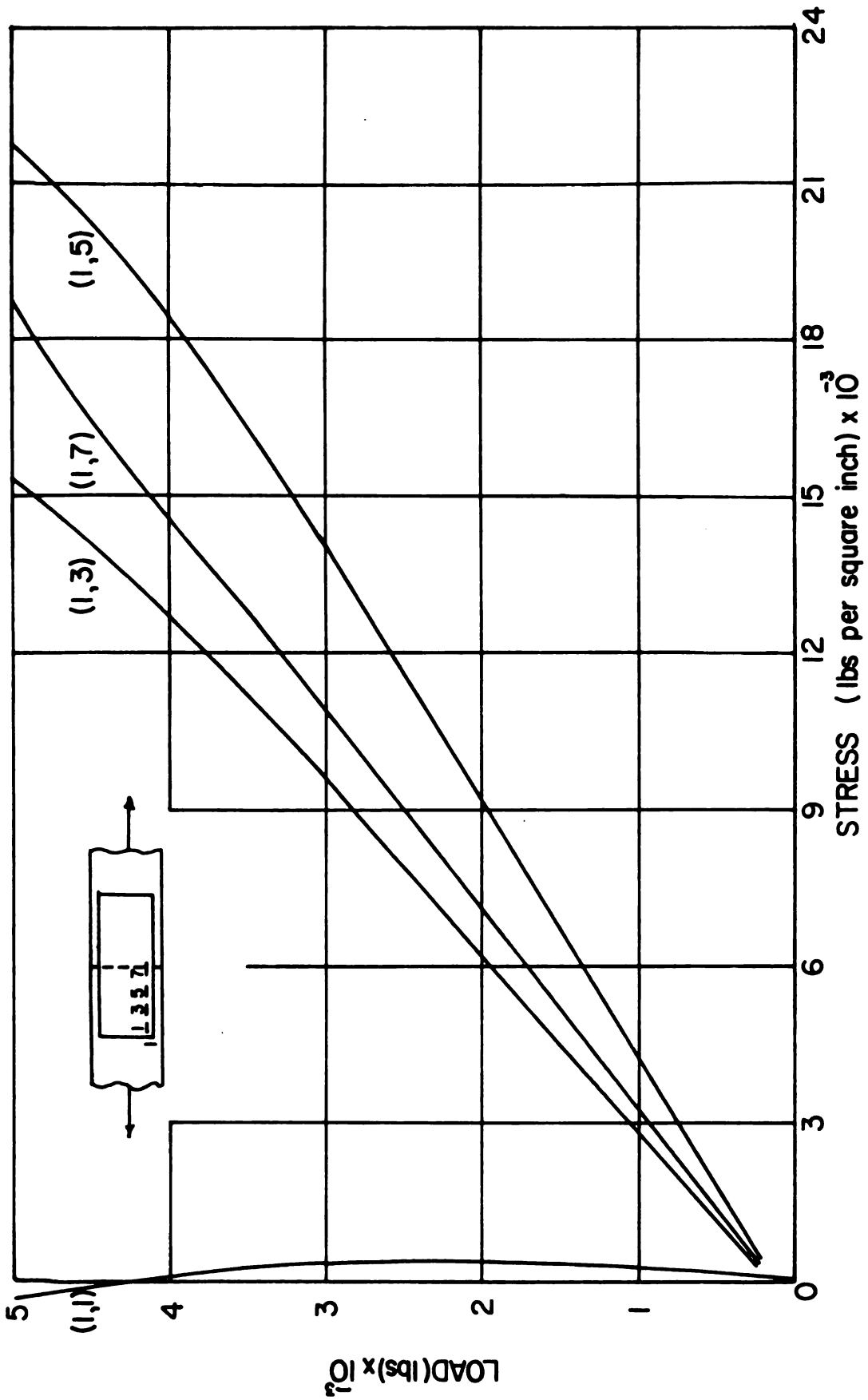


FIG. 14 LOAD STRESS CURVES FOR POINTS (1,1), (1,3), (1,5) AND (1,7)

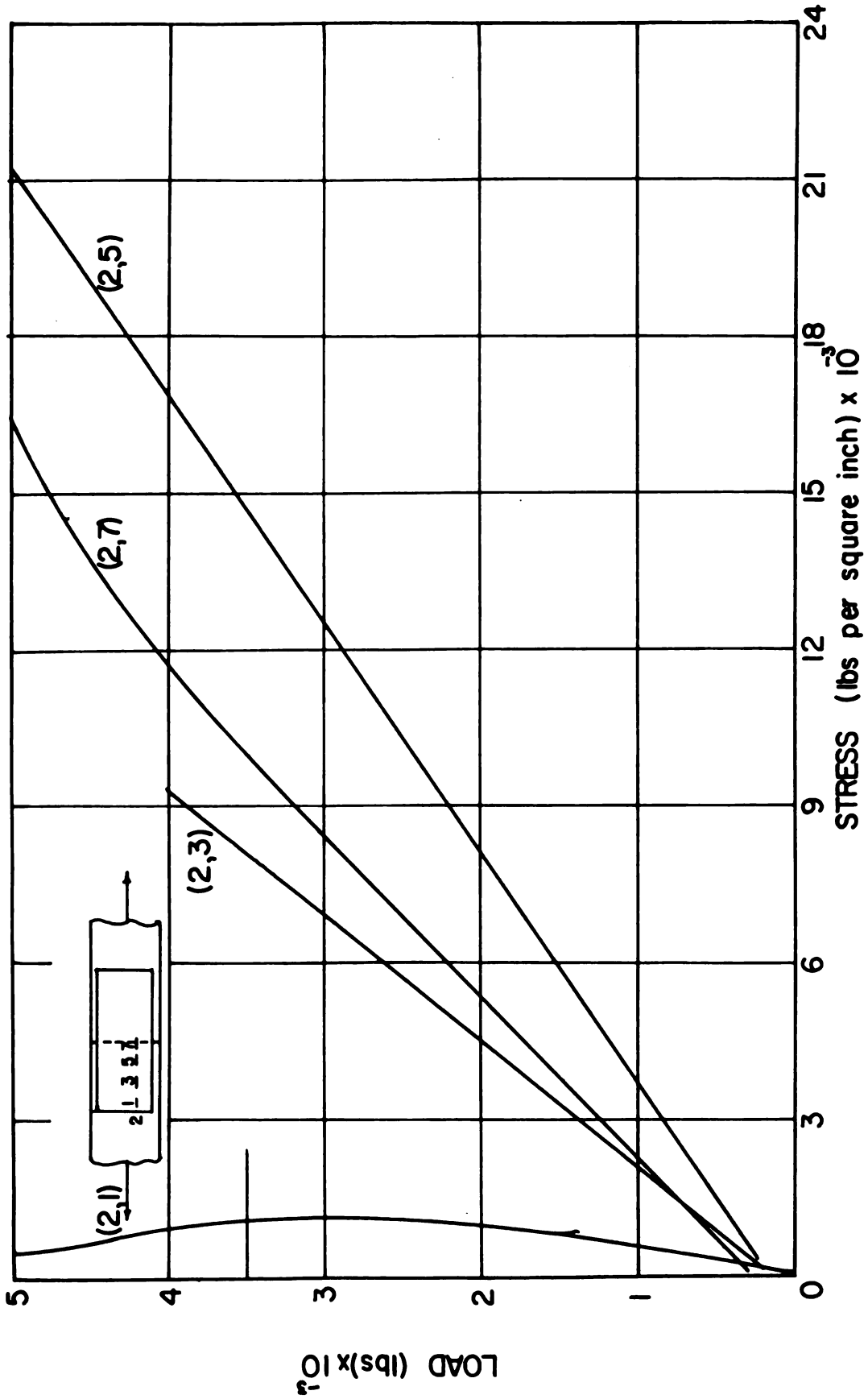


FIG. 15 LOAD STRESS CURVES FOR POINTS (2,1), (2,3), (2,5) AND (2,7)

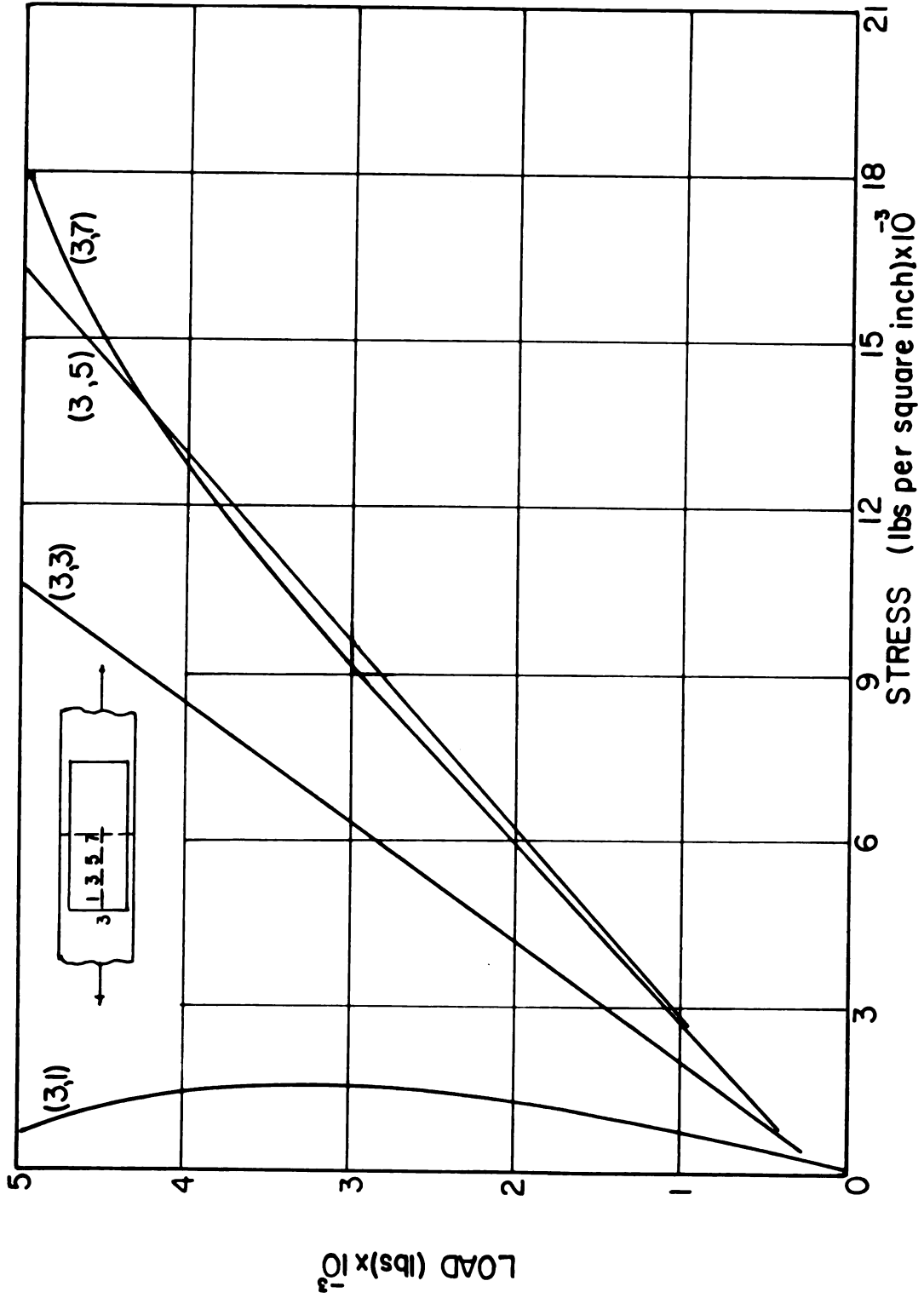


FIG. 16 LOAD STRESS CURVES FOR POINTS (3,1), (3,3), (3,5) AND (3,7)

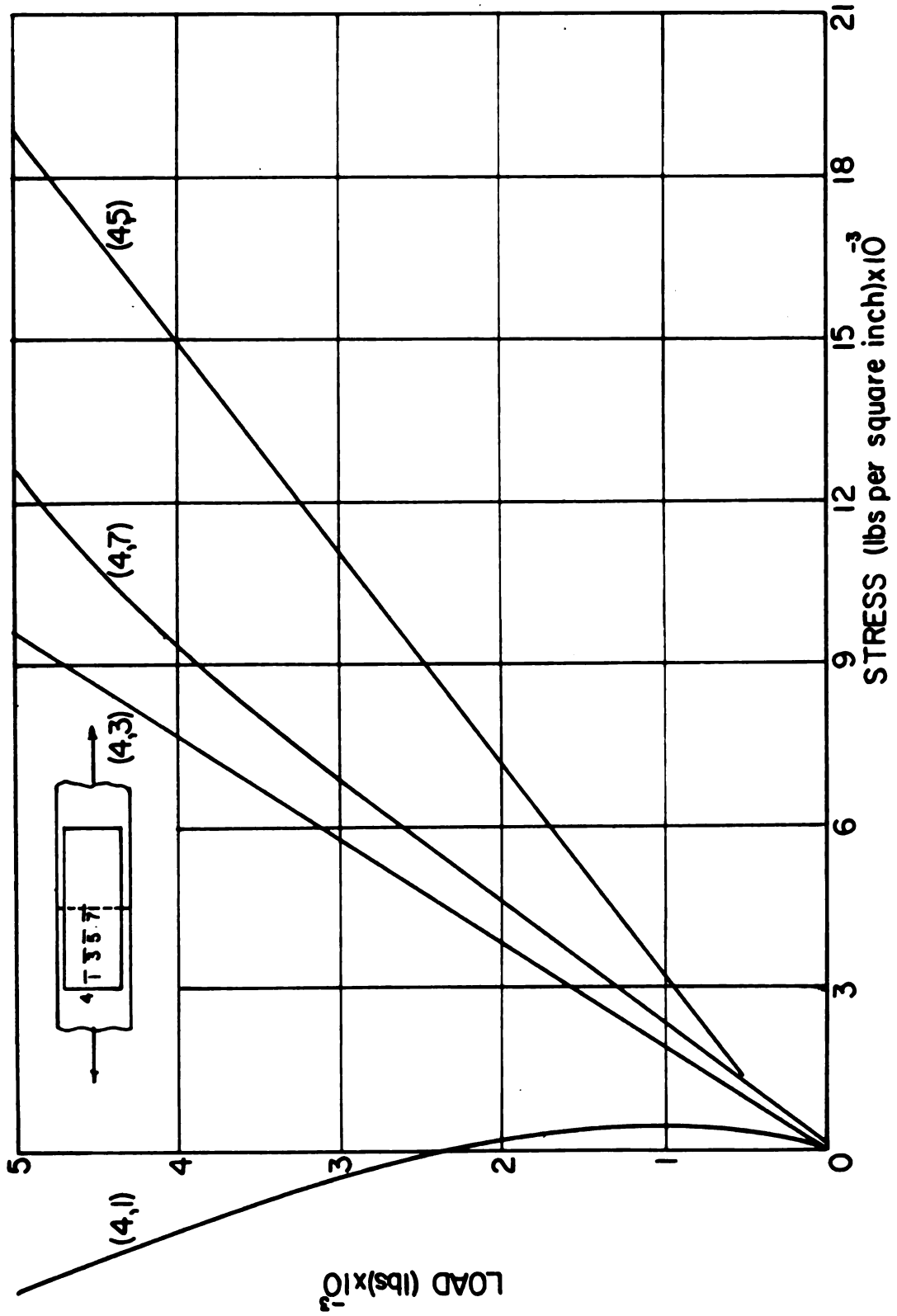


FIG. 17 LOAD STRESS CURVES FOR POINTS (4,1), (4,3), (4,5), AND (4,7)

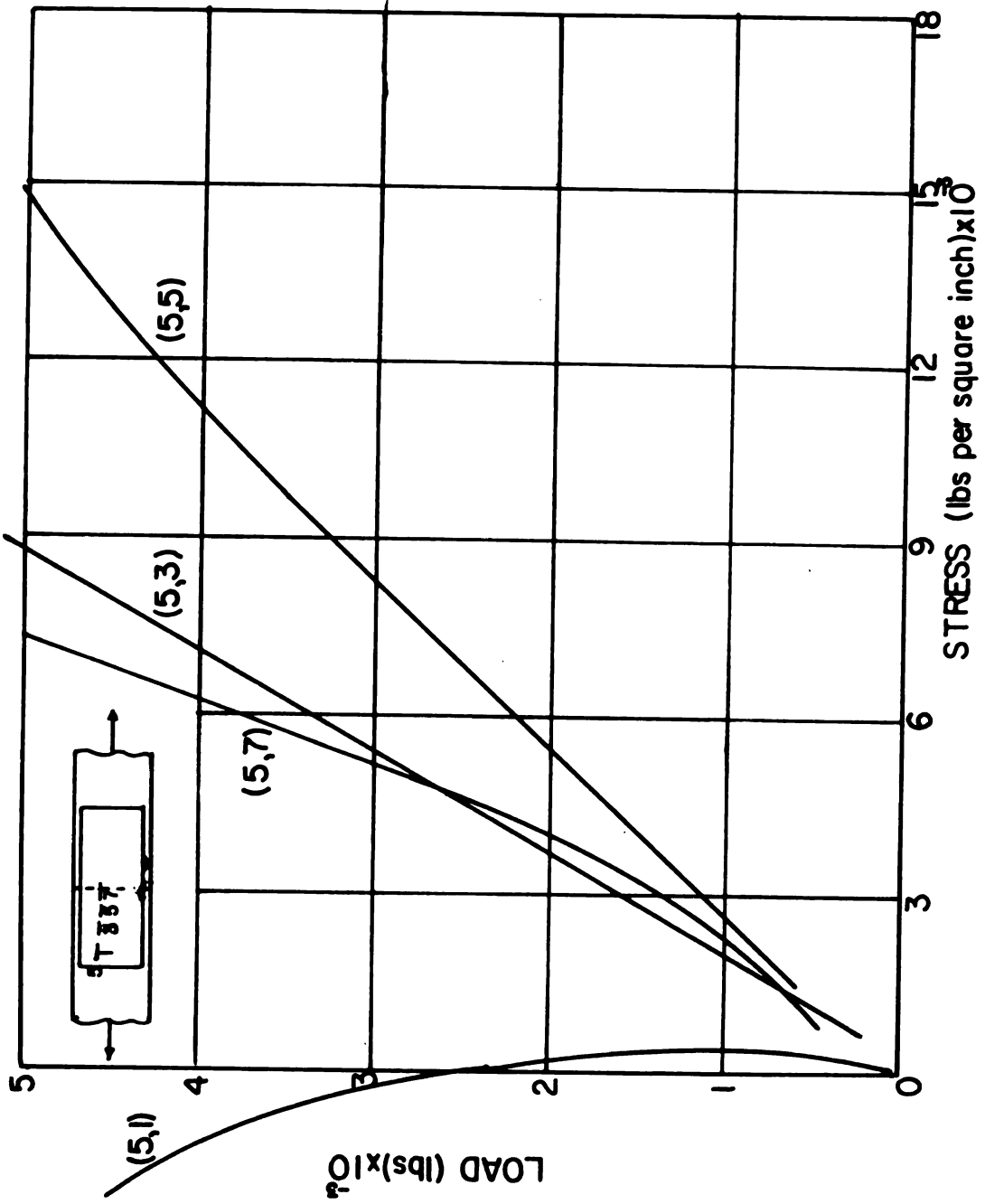


FIG. 18 LOAD STRESS CURVES FOR POINTS (5,1), (5,3), (5,5) AND (5,7)

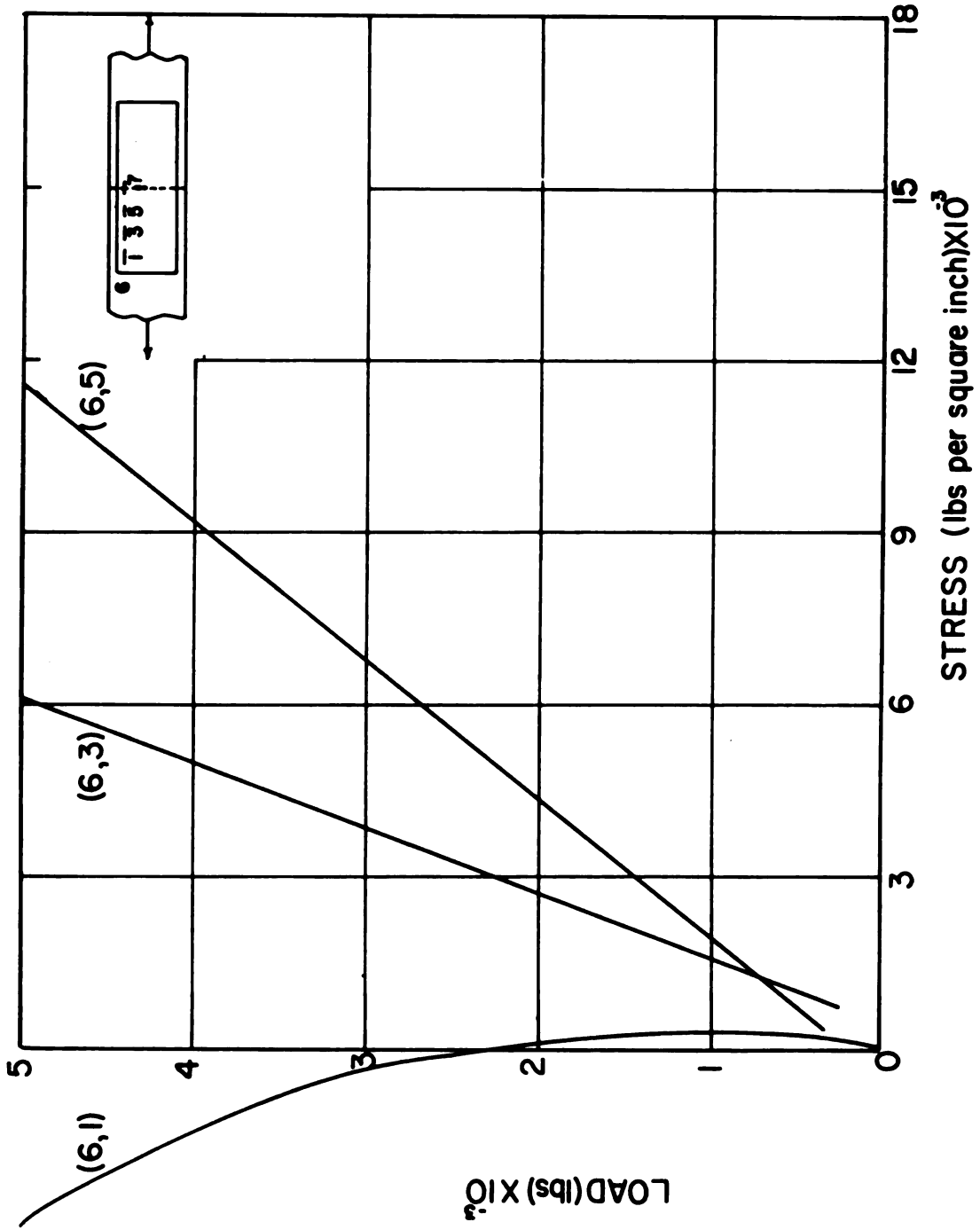


FIG. 19 LOAD STRESS CURVES FOR POINTS (6,1), (6,3), (6,5)

are discussed here, as very close agreement in stress distribution existed between the two tests. Figures 20 and 21 present the same data in two different ways as obtained from the wire-type gages. Figure 20 shows the stress variation along four different rows as indicated. Each row, normal to the direction of loading, consisted of a set of six gages. The first set at the end of the connector indicated very small strains which were in tension for smaller loads and became compressive for higher loads. This was attributed to the warping tendency of the metal plate as the load was increased.

Figure 21 shows the same data as presented in Figure 20 except that the stress plot is made at six different columns along the direction of loading. This plot indicates the existence of eccentric loading in testing which in most tension tests is unavoidable. The stresses varied from maximums along column one to minimums along column six.

The stresses obtained from the strain measurements by foil-type gages mounted at the bases of the miniature cantilever teeth are presented in Figures 22 and 23. Here also the stresses increase gradually from minimum near the ends to maximum along the third row. It is also apparent from these curves that teeth along the sides of the joint take comparatively less stress.

A special note should be made here of different scales used in representing the stresses as obtained from wire-type and foil-type gages. Generally, the stresses at the bases of cantilever teeth were higher than those at the corresponding strips.

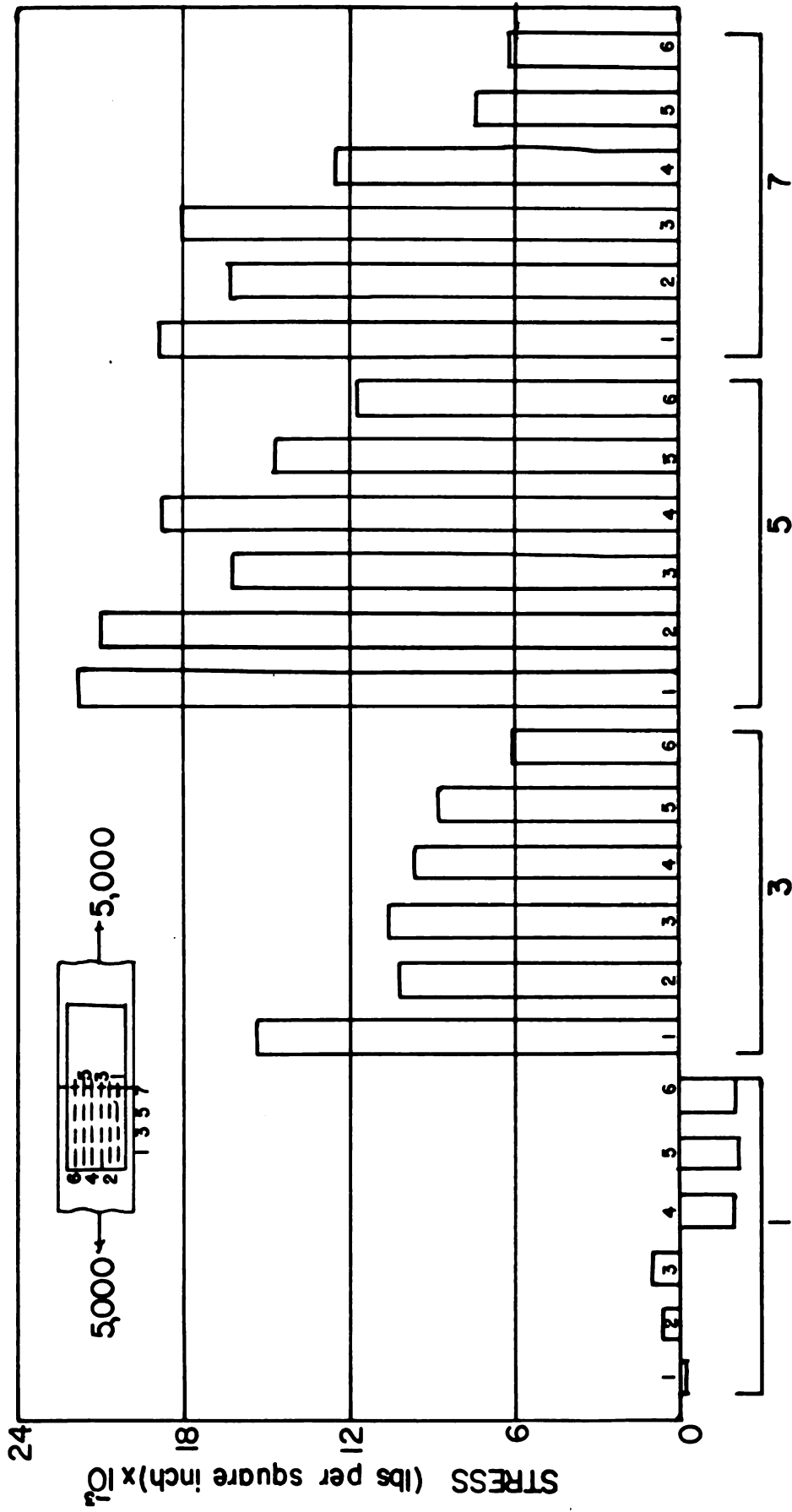


FIG. 20 STRESS DISTRIBUTION IN THE METAL-PLATE CONNECTOR AT 5,000 LBS TENSION



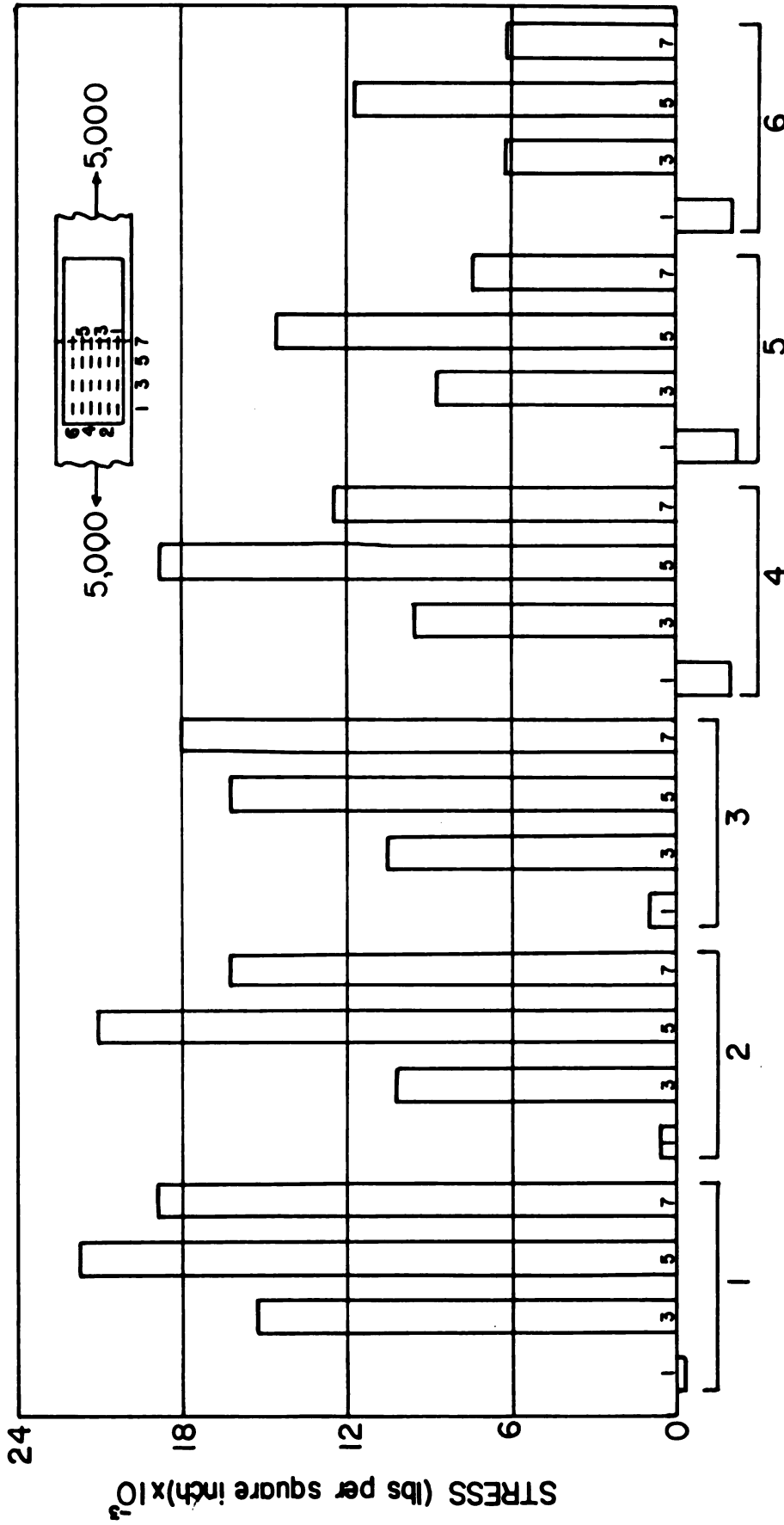


FIG. 21 STRESS DISTRIBUTION IN THE METAL-PLATE CONNECTOR AT 5,000 LBS TENSION

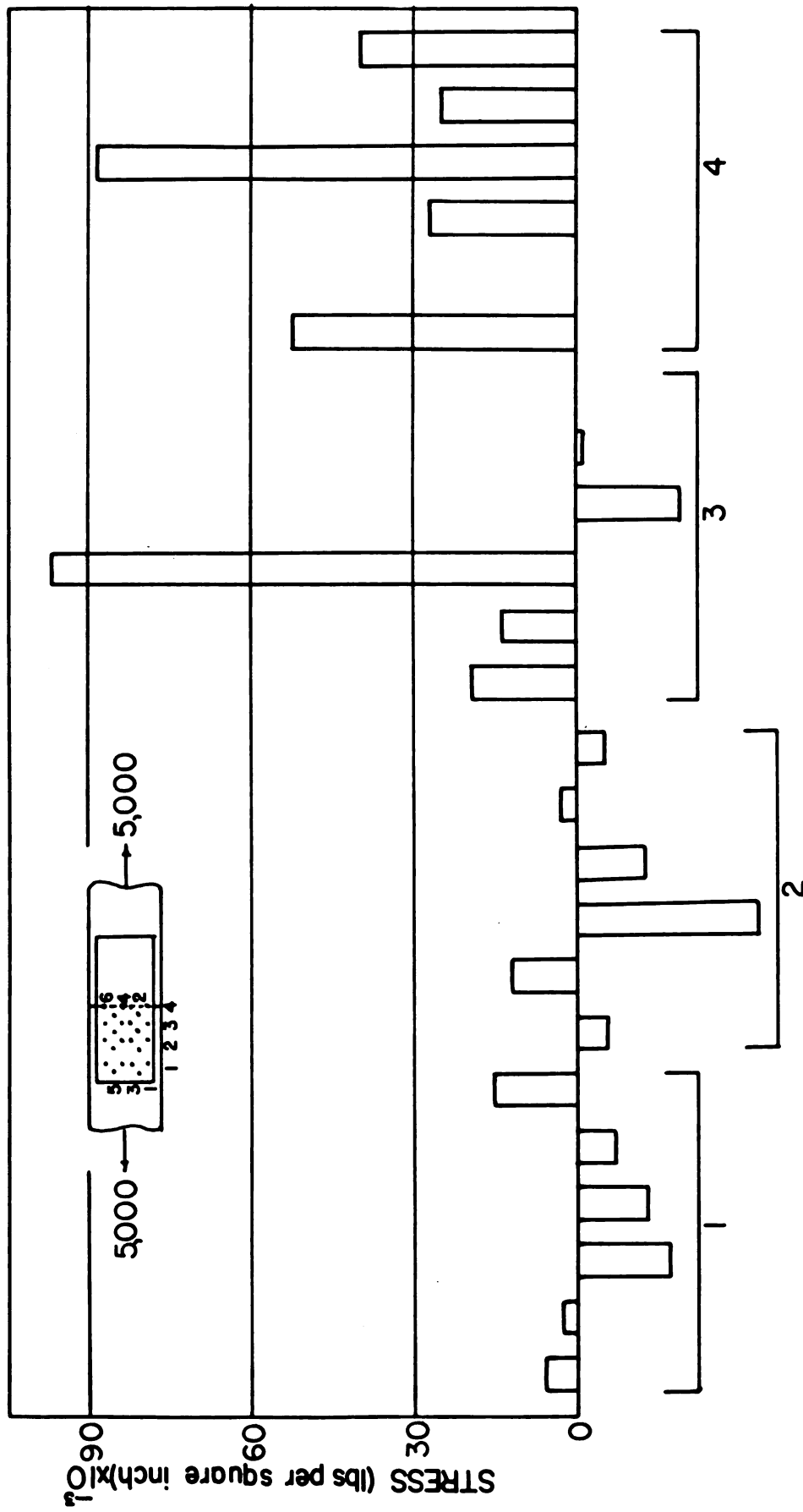


FIG. 22 STRESSES AT THE BASES OF CANTILEVER TEETH IN THE METAL-PLATE CONNECTOR AT 5,000 LBS TENSION

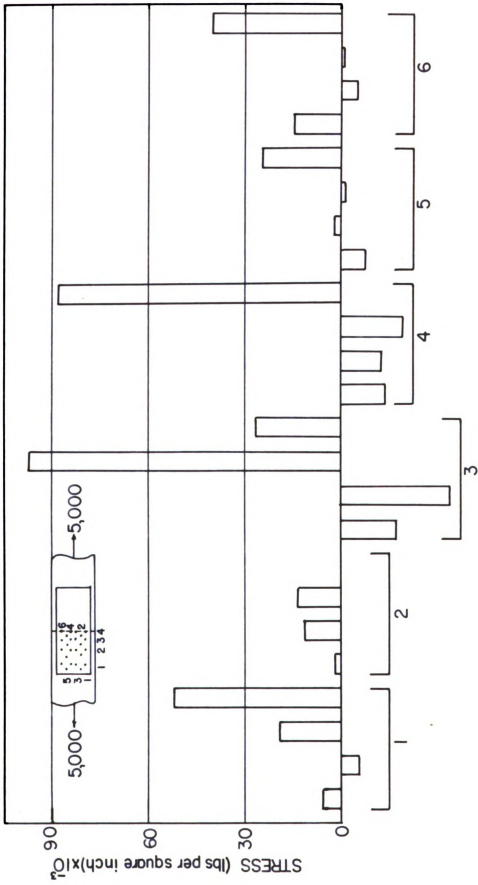


FIG. 23 STRESSES AT THE BASES OF CANTILEVER TEETH IN THE METAL-PLATE CONNECTOR
AT 5,000 LBS TENSION

RESULTS AND DISCUSSION

Comparison of Theoretical and Experimental Results

The results of the Difference Equation solution for the no-slip case are presented in Figure 24. A set of average experimental points as obtained by strain gage measurements at four different locations along the connector are also shown. Theoretical curve for the stress in the connector increases from zero at $x = 0$ to a maximum at $x = L$.

The experimental points are widely scattered on both sides of the theoretical curve. This probably can be expected as the analysis is only an approximation to the actual behavior of the joint. A part of this discrepancy might be attributed to the facts that the joint is not rigid as has been assumed but semi-rigid and that the friction between connectors and wood, grain orientations of wood, and moisture content of wood have not been considered.

It must also be mentioned here, however, that a difference equation assuming equal slip of all the teeth in the connector was derived and solved in a similar way. The slip function was obtained by fitting a least squares polynomial to a set of experimental points obtained from load-gross slip tests. The result of this consideration, however, did not improve the analysis, but on the contrary predicted rather absurd results. This probably was due to the erroneous assumption that each connector slips the same amount. Actually the connectors do not exert the same force on the wood and hence the slip is not the same for each connector.

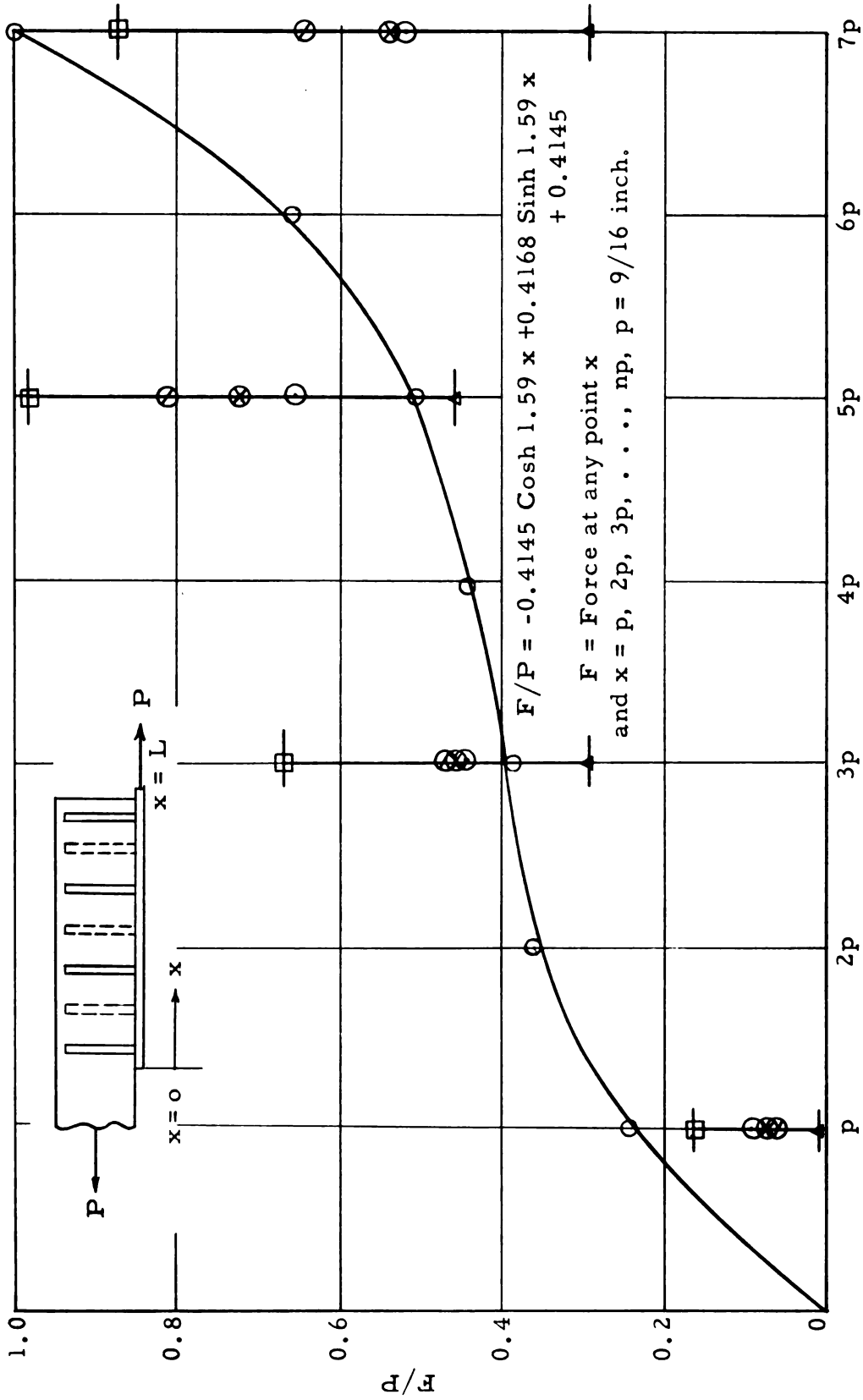


Fig. 24. Comparison of experimental and theoretical results as predicted by the difference equation solution.

The theoretical curve obtained from the analysis of the principle of minimum complementary energy is shown in Figure 25. The equation obtained by this analysis for the normal stress σ_c at any point in the connector was

$$\frac{\sigma_c}{P} = -1.875 \text{ Cosh } 1.155 x + 1.94 \text{ Sinh } 1.155 x + 1.875$$

Four sets of readings as obtained by strain gage measurements are also shown. These points are plotted from the strain gage data taken randomly at different loads and averaged over each row. Here again the experimental points are widely scattered on both sides of the curve. The interesting point to note, however, is that even with the idealized assumptions that had been made in carrying out this analysis, it gives results that are not too much different from those obtained by strain gage measurements.

It is, of course, clear from Figure 25 that the stresses in the metal plate are not uniform as assumed in normal design practices. The maximum calculated stress was 2.4 times the average stress.

The theoretical curves in both cases predicted the maximum stress in the middle of the joint, however, the experimental readings gave the maximum at the second gage point from the middle (row five). This was true only up to a certain load. As the load was increased up to the ultimate, it was observed that the maximum stress did occur in the middle. This could have been due to the relaxation in the load transferring characteristics of such connectors. Since the fourth row of the connectors are not as properly imbedded into the wood (because of their proximity to the end of the wood pieces) as are the rest of the connectors, this row would be more susceptible to slip than the rest. Consequently, it would not be able to take its full share of the load. But as the load is increased to a certain value near the ultimate, the slip progresses from the middle towards the end. Thus the stress in middle row eventually becomes more than the one next to it.

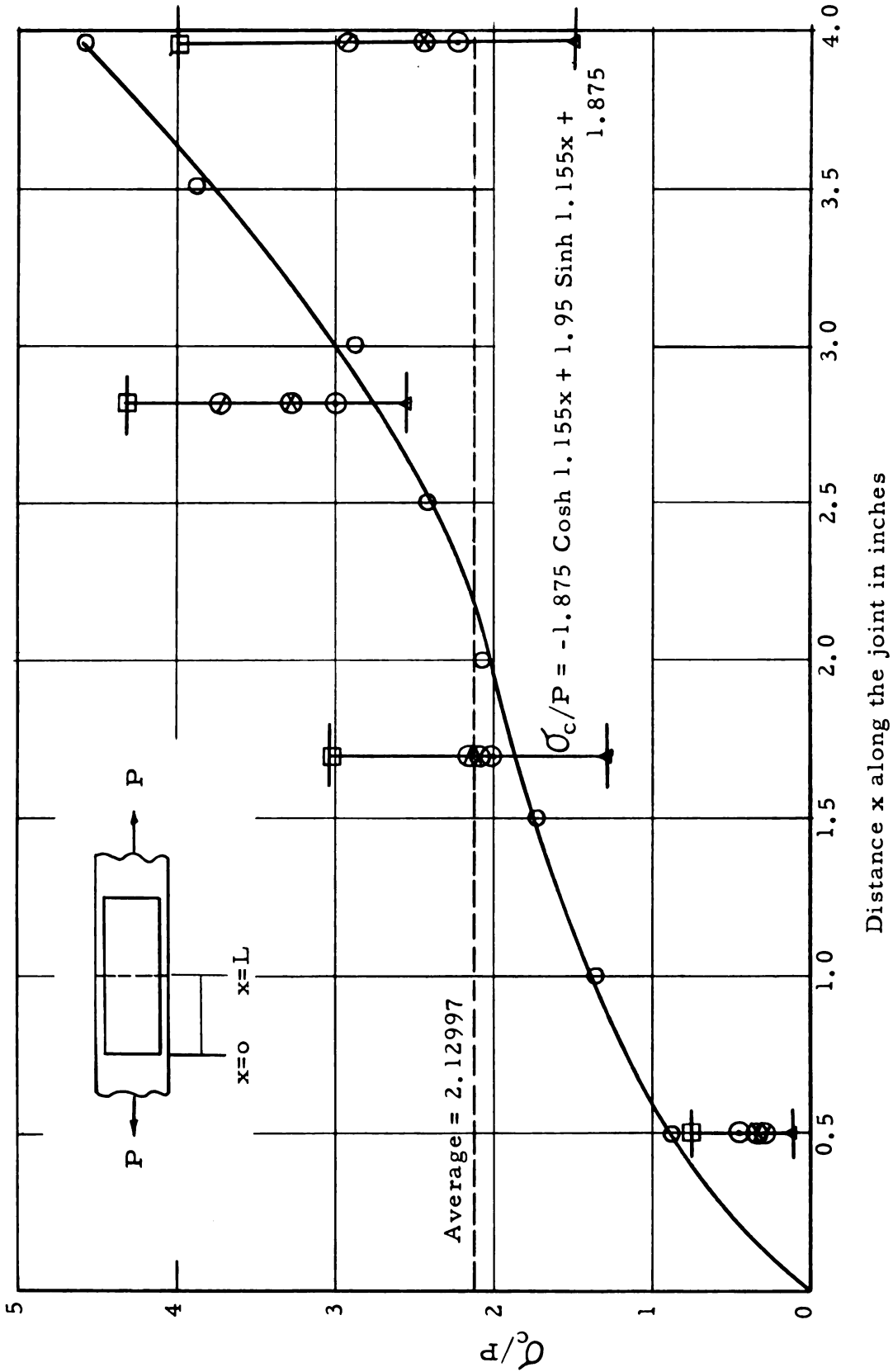


Fig. 25. Comparison of experimental and theoretical results as predicted by the principle of minimum complementary energy.

The results of both of the theoretical analyses are plotted in Figure 26. It is interesting to note that both theoretical curves are rather close and predict a similar stress distribution. The equation of the result predicted by difference equation solution was

$$\frac{\sigma_c}{P} = -0.04526 \text{ Cosh } 1.59 x + 0.04551 \text{ Sinh } 1.59 x + .04526$$

while that predicted by the principle of minimum complementary energy was

$$\frac{\sigma_c}{P} = -1.875 \text{ Cosh } 1.155 x + 1.94 \text{ Sinh } 1.155 x + 1.875$$

It must be emphasized here that these equations are applicable only within the elastic range. Their use, therefore, must be limited to this range.

The maximum calculated stress, which occurred in the middle was 2.4 times the average stress. A more uniform stress distribution might be obtained by not punching the middle row and reducing the length of the connectors with a proportionate increase in their number.

Evaluation of PhotoStress Analysis

The results of the PhotoStress analysis as presented in Table I and Figures 9, 10 and 11 for a uniaxial load of 5,000 lbs indicated that the stress in the metal plate has a rather sharp stress gradient. The principal stress difference varied from a maximum of 46,000 psi at the center row to a minimum of 14,810 psi closer to the ends.

An approximate separation of the principal stresses when compared with the calculated stresses at the middle row indicated a wide variation (9.61 to 42.20%) between the measured and the calculated values. This variation was jointly accounted for by stress gradient effect, stress concentration effect, experimental error and possible variation in the E and μ values of the plate.

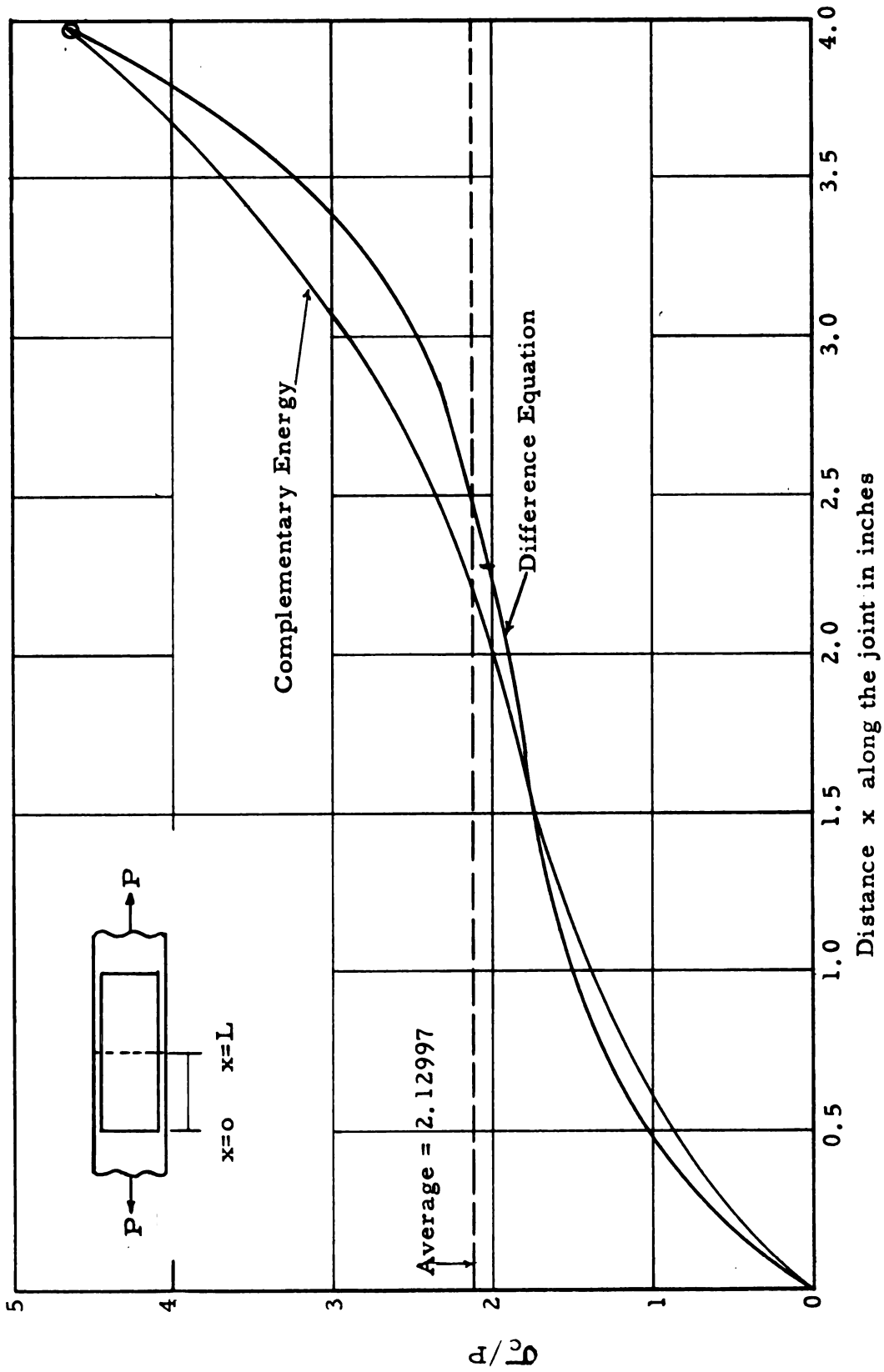


Fig. 26. Stress distribution in the metal plate connector as obtained from the analyses of the minimum complementary energy and the difference equation.

The direction of the principal stresses at the central unpunched strips were in close agreement with the expectation. However, they were rather complicated, away from the center. A number of points in hydrostatic state were also observed. The magnitude of the stresses and their directions were found symmetrical about the axis of loading.

For PhotoStress analysis to be really effective as a tool of stress analysis in a multiconnected body of intricate shapes, experimental separation of principal stresses seems to be highly desirable. For this purpose an oblique incidence meter is a necessity.

SUMMARY

The main objective of this study was to conduct a theoretical and experimental investigation of stress distribution in a metal-plate-connected timber joint.

The theoretical investigation consisted of two different methods. One utilized the discrete approach of a Difference Equation while the other used the continuous approach of the principle of minimum complementary energy.

A second order difference equation was derived and solved for a general case. The results for a particular case of the metal plate connector were calculated and plotted together with experimental results for comparison.

The principle of minimum complementary energy was used to derive a second order ordinary linear differential equation for an idealized case. The metal plate connector was treated as if glued to the surface of the wood by a fictitious adhesive of negligible thickness. The differential equation thus obtained was solved with appropriate boundary conditions. The results for a particular case of metal plate connector were plotted for comparison with the experimental results.

Two different methods of experimental stress analysis were used; namely, PhotoStress analysis and a strain gage technique. The PhotoStress analysis provided, qualitatively, the overall pattern of stress distribution in the entire plate. A set of bar graphs for the principal stress difference ($\sigma_1 - \sigma_2$) along the various rows of teeth in the metal plate connector were plotted. A symmetrical stress distribution was obtained. The isoclinic pattern for a portion of the plate was thoroughly examined. From this isoclinic pattern stress trajectories were drawn.

The strain gage technique was used to obtain accurate and reliable values of strain in the metal plate to verify the theoretical results.

The particular results of both of the theoretical analyses predicted reasonable agreement with the experimental values, and similar patterns of stress distribution. The maximum stress as calculated by complementary energy method was 2.4 times the average stress.

The general results of the difference equation solution can be used to calculate stresses in metal plate connectors as well as riveted and bolted joints. Similarly, the results of complementary energy method can be used to calculate stresses in metal plate connector as well as in adhesive and welded joints.

CONCLUSIONS AND OBSERVATIONS

The following conclusions and observations are based on the results of this investigation.

1. The results of the difference equation solution as well as that of the principle of minimum complementary energy predict reasonable agreement with the experimental results. Either method can be used to calculate stresses in the metal plate connector.
2. The difference equation solution can also be used with at least equal accuracy for riveted and bolted joints. Similarly the results of the principle of minimum complementary energy are equally applicable to adhesive as well as welded joints.
3. The stresses in the metal plate are not uniform as assumed in the normal design practices. The maximum calculated stress in the connector was 2.4 times the average value.
4. A set of distruction tests made in tension resulted in tearing failure of the plate in the center of the joint. If the middle part of the plate were not punched, the strength of the joint should be greater and also a more uniform stress distribution should result.
5. The PhotoStress analysis provided an overall pattern of stress distribution in the entire plate. The variation between measured and calculated principal stress difference ranged from 9.6% to 42.2%. The results of this analysis were, however, incomplete as the shape of the punched plate was too complicated for analytical separation of the principal stresses. The equipment for experimental separation (oblique incidence meter) was not available.

SUGGESTIONS FOR FURTHER STUDY

1. Carry out theoretical analysis using Plastic Analysis by assuming a criterion of yielding and a mechanism of hinge formation.
2. Determine the dynamic behavior of the joint under different cycles of loading and aging.
3. Establish long term aging characteristics of such joints.

REFERENCES

1. Boyd, J. S. (1954). Secondary Stresses in Trusses with Rigid Joints, Special Application to Glued Wooden Trusses. Ph. D. thesis Iowa State Univ. (unpublished).
2. Boyd, L. L. (1959). Design of Semi-Rigid Timber Joints. A. S. A. E. Paper No. 59-828, presented at 1959 Annual Meeting.
3. Brown, H. P., A. J. Panshin and C. C. Forsaith (1952). Text Book of Wood Technology, Vol. II. McGraw-Hill Book Co., Inc., New York.
4. Duffy, J. (1961). Effects of the thickness of birefringent coatings, pp. 74-82. Experimental Mechanics, March 1961.
5. Durelli, A. J., E. A. Phillips and C. H. Tsao (1958). Introduction to the Theoretical and Experimental Analysis of Stress and Strain. McGraw-Hill Book Co., New York.
6. Felton, K. E. and H. D. Bartlett (1963). Punched Metal Truss Plates Used in Timber Joints. A. S. A. E. Paper No. 63-431, presented at 1963 Annual Meeting.
7. Freudenthal, A. M. (1950). The Inelastic Behavior of Engineering Materials and Structures. John Wiley and Sons Inc., New York.
8. Frocht, M. M. (1941). Photoelasticity, Vol. I. John Wiley and Sons Inc., New York.
9. Goldberg, S. (1958). Introduction to Difference Equations. John Wiley and Sons Inc., New York.
10. Granholm, H. (?). A Summary of Report on Composite Beams and Columns with Particular Regard to Nailed Timber Structures.
11. Harris, C. O. (1962). The Analysis of a Parallel-Type Structural Connection by Means of a Difference Equation. Unpublished manuscript.

12. Hetenyi, M. (1950). Handbook of Experimental Stress Analysis. John Wiley and Sons Inc., New York.
13. Hoff, N. J. (1956). The Analysis of Structures. John Wiley and Sons, Inc., New York.
14. Hrennikoff, A. (1932). Work of Rivets in Riveted Joints. Am. Soc. of Civil Engineers Proceedings Nov. 1932.
15. Joy, F. A. (1961). Methods for Testing Metal Connector Plates Used in Trussed Rafter Construction. Engineering Experiment Dept., Penn. State Univ.
16. Kuhn, Paul (1956). Stresses in Aircraft and Shell Structures. McGraw-Hill Book Co., Inc., New York.
17. Muckle, W. (1949). The distribution of Load in Riveted Joints. The Shipbuilder and Marine Engine-Builder, pp. 225-228, April 1949.
18. Post, D. and F. Zandman (1961). Accuracy of Birefringent Coating Method for Coating Arbitrary Thicknesses, pp. 21-32. Experimental Mechanics. Jan. 1961.
19. Zandman, F. (1959). PhotoStress Principles and Applications. Instruments Division, The Budd Company.

MICHIGAN STATE UNIVERSITY LIBRARIES



3 1293 03169 7810